Available online at www.sciencedirect.com

ScienceDirect

Geochimica et Cosmochimica Acta 142 (2014) 458–481

Geochimica et Cosmochimica Acta

www.elsevier.com/locate/gca

The effects of diagenesis and dolomitization on Ca and Mg isotopes in marine platform carbonates: Implications for the geochemical cycles of Ca and Mg

Matthew S. Fantle [a,*], John Higgins [b]

[a] Department of Geosciences, Pennsylvania State University, University Park, PA 16802, United States
[b] Department of Geosciences, Princeton University, Princeton, NJ 08544, United States

Received 25 March 2014; accepted in revised form 29 July 2014; available online 10 August 2014

Abstract

The Ca, Mg, O, and C isotopic and trace elemental compositions of marine limestones and dolostones from ODP Site 1196A, which range in depth (~58 to 627 mbsf) and in depositional age (~5 and 23 Ma), are presented. The objectives of the study are to explore the potential for non-traditional isotope systems to fingerprint diagenesis, to quantify the extent to which geochemical proxies are altered during diagenesis, and to investigate the importance of diagenesis within the global Ca and Mg geochemical cycles. The data suggest that Ca, which has a relatively high solid to fluid mass ratio, can be isotopically altered during diagenesis. In addition, the alteration of Ca correlates with the alteration of Mg in such a way that both can serve as useful tools for deciphering diagenesis in ancient rocks.

Bulk carbonate $\delta^{44}Ca$ values vary between 0.60 and 1.31‰ (SRM-915a scale); the average limestone $\delta^{44}Ca$ is 0.97 ± 0.24‰ (1SD), identical within error to the average dolostone (1.03 ± 0.15 1SD ‰). Magnesium isotopic compositions ($\delta^{26}Mg$, DSM-3 scale) range between −2.59‰ and −3.91‰, and limestones (-3.60 ± 0.25‰) and dolostones (-2.68 ± 0.07‰) are isotopically distinct. Carbon isotopic compositions ($\delta^{13}C$, PDB scale) vary between 0.86‰ and 2.47‰, with average limestone (1.96 ± 0.31‰) marginally offset relative to average dolostone (1.68 ± 0.57‰). The oxygen isotopic compositions ($\delta^{18}O$, PDB scale) of limestones (-1.22 ± 0.94‰) are substantially lower than the dolostones measured (2.72 ± 1.07‰).

The isotopic data from 1196A suggest distinct and coherent trends in isotopic and elemental compositions that are interpreted in terms of diagenetic trajectories. Numerical modeling supports the contention that such trends can be interpreted as diagenetic, and suggests that the appropriate distribution coefficient (K_{Mg}) associated with limestone diagenesis is ~1 to 5×10^{-3}, distinctly lower than those values (>0.015) reported in laboratory studies. With respect to Mg isotopes, the modeling also suggest that diagenetic fractionation factors of ~0.9955 (−4.5‰) and 0.9980 (−2‰) are appropriate for limestone diagenesis and dolomitization, respectively.

1. INTRODUCTION

The question of seawater chemical evolution, and the utility of seawater chemistry for elucidating the functioning of the Earth system, has been of fundamental interest to geoscientists for centuries (e.g., Boyle, 1674; Halley, 1714; Joly, 1899; Clarke, 1911; Conway, 1943; Rubey, 1951; Sillen, 1961, 1963; Holland, 1965; Walker and Scott, 1966; Broecker, 1971; Holland, 2005). The relevance of elucidating the history of seawater chemistry and the processes that control it cannot be understated, as seawater chemical composition (1) is a reference against which we can evaluate

* Corresponding author. Tel.: +1 814 863 9968; fax: +1 814 863 7823.
E-mail address: mfantle@psu.edu (M.S. Fantle).

http://dx.doi.org/10.1016/j.gca.2014.07.025
0016-7037/

models of the global carbon cycle on geologic time scales, and (2) directly affects the manner in which we interpret paleo-seawater surface temperature proxies (e.g. Mg/Ca) and variations in the mineralogy of marine carbonates over Earth history. The significance of seawater evolution was nicely put into context more than sixty years ago by Rubey (1951), who stated that the "...question (of seawater evolution) ramifies almost endlessly into nearly every fundamental problem of Earth history and far beyond....". Accordingly, constraining (and interpreting) seawater chemical evolution is a primary objective of geosciences research.

With the emergence of so-called "non-traditional" stable isotope systems over the past fifteen years, the focus on seawater chemical evolution has taken on a new dimension. As the ability to measure the isotopic composition of major cations such as Ca, Mg, K, and Si has emerged, so too has the potential to trace the geochemical cycles of these elements. Not only do metal isotopes provide additional tools for investigating what is typically an underdetermined system, but the cycles of these elements are intimately coupled to the carbon cycle, an important driver of climate through silicate weathering and the burial of carbonate minerals. In addition, elements such as Ca and Mg provide direct constraints on the origins and diagenetic history of marine carbonate minerals – one of the most widely used proxy archives for constraining past environment and climate.

Metal isotopes have potential as geochemical proxies to reveal fundamental aspects of the Earth system, and responses to perturbations, over a range of time scales. Calcium isotopes, for instance, have been suggested as a geochemical proxy for sea surface temperature (Nägler et al., 2000; Gussone et al., 2005; Langer et al., 2007) as well as a tool for reconstructing Ca cycling in the geologic past (De La Rocha and DePaolo, 2000; DePaolo, 2004; Fantle and DePaolo, 2005; Fantle, 2010). Magnesium isotopes may provide unique insights into the diagenetic history of carbonate minerals (Fantle and Teng, 2012; Higgins and Schrag, 2012) and the origins of marine dolomite (Higgins and Schrag, 2010), and may serve as a tool for reconstructing the global Mg cycle over geologic time scales (Tipper et al., 2006). At present our understanding of the utility of these new isotopic systems for elucidating global geochemical cycles and Earth history is limited, in part by a lack of data on how these systems are affected by diagenesis. Studies of Ca and Mg isotope variability associated with diagenesis are therefore integral to proxy development, and may provide new approaches to identifying diagenetic effects in ancient marine carbonates.

First and foremost, the fidelity (and ultimate utility) of any proxy depends on the extent to which diagenesis alters initial isotopic compositions. Diagenetic alteration is affected by the recrystallization rate of the solid (R), the extent of isotopic disequilibrium between the solid and fluid ($(\delta_s - \delta_f) - \Delta^{diag}_{s-f}$), and time (Fantle and DePaolo, 2007; Fantle et al., 2010):

$$d\delta_s = -R\left[(\delta_s - \delta_f) - \Delta^{diag}_{s-f}\right]dt \quad (1)$$

These factors are influenced by additional system parameters, such as the fluid advection velocity and aqueous chemistry (e.g., saturation state). Most important is the extent to which the system is open or closed, a condition expressed by parameters such as the advective reaction length scale (L_a; Fantle et al., 2010). In cases where the system is effectively closed, diagenesis will cause no changes in the proxy over the advective reaction length scale. Redistribution of elements and reequilibration can, and likely does, still occur but the effects are limited over relatively small length scales. Such a scenario is likely for major elements in the reacting solid phase (Ca, C, and O), which have relatively small L_a's compared to trace constituents (e.g., Sr, Mg, and B). On the other hand, when the advective reaction length is large, the effect of advection is to maintain the solid well out of equilibrium with the fluid ($(\delta_s - \delta_f) - \Delta^{diag}_{s-f} > 0$). As a result, the system is open and the solid can be substantially altered.

Early work based on numerical modeling of Sr geochemistry in carbonate ooze sediments indicated that the total amount of integrated diagenetic reaction over 20 Ma was on the order of 15–25% (Richter and DePaolo, 1987, 1988; Richter and Liang, 1993; Richter, 1996). More recent work suggests that reaction rates may be as much as 10–20 times higher than previously supposed (Fantle and DePaolo, 2007). Equally high silicate dissolution rates have been noted in siliciclastic marine sections by measuring and modeling uranium isotopes (Maher et al., 2004, 2006). Consideration of such rates in the sedimentary column implies that, over a period of 35 Ma, carbonates may be more than 60% recrystallized. There is also good evidence to suggest that the Ca isotopic fractionation factor ($\alpha_{s\text{-}f}$) associated with marine diagenesis is close to one (Fantle and DePaolo, 2007), which is substantially different from the fractionation factor associated with carbonate formation ($\alpha \sim 0.9986$) and therefore provides leverage to alter the isotopic composition of the solid. Similarly, Mg isotope fractionation associated with calcite recrystallization in deep-sea carbonate sediments ($\alpha \sim 0.996$; Higgins and Schrag, 2012) appears to be significantly larger than Mg isotope fractionation factors observed in seeded laboratory precipitation experiments (Mavromatis et al., 2013).

The current work is motivated by questions surrounding the fidelity of the Ca and Mg isotope proxies and the dominant processes that control the evolution of seawater chemistry over geologic time scales. The relevant questions are: (1) what are the isotopic compositions of the primary output fluxes from the ocean? Specifically, what is the isotopic composition of marine limestone and dolomite and how does dolomite compare to shallow water carbonates? (2) What is the fractionation factor associated with dolomite formation in a diagenetic setting? Given that dolomite precipitation is difficult to study in experimental settings at geologically-relevant rates, natural samples must form the basis for such work. And, finally, (3) to what extents are the Ca and Mg isotopic compositions of shallow water carbonates altered during diagenesis? Does a multi-proxy perspective elucidate significant and decipherable trends that allow for the identification of diagenetic alteration in ancient sediments?

The current study utilizes isotopic measurements of Ca, Mg, O, and C, in addition to elemental ratios, to inform these questions. The study analyzes altered platform carbonates (limestones and dolostones) from ODP Site 1196A, and interprets the isotopic trends in terms of diagenetic alteration. The implications of the data are discussed in the context of a diagenetic box model and the significance for the global Ca and Mg cycles presented.

2. SITE DESCRIPTION

Geochemical data are presented for samples collected during Ocean Drilling Project Leg 194, Site 1196 (21°0.371′S, 152°51.512′E; Fig. 1a), which is located on the northern edge of the Southern Marion Platform about 20 km east of the Great Barrier Reef margin (Isern et al., 2002). Hole 1196A was drilled in 304 meters water depth, from 0 to 672.2 meters below seafloor (mbsf; Isern et al., 2002).

Hole 1196A contains Miocene limestones and dolostones, which are underlain by upper Oligocene phosphate-rich siliciclastics (sandstone, claystone, and phosphatic sands; Isern et al., 2002). Coralline red algae fossils dominate most of the section. Between 0 and ~182 mbsf, the sediments are composed of dolomitic floatstone and rudstone (Fig. 1b). Within this unit occur rhodoliths and coral fragments in a matrix of benthic foraminifera, red algae, and mollusks. Isern et al. (2002) note that dolomitization is not pervasive in the upper part of this unit (0 to ~117 mbsf). The identified sub-unit below (~117 to 126 mbsf) is characterized by a greater degree of dolomitization (though rock texture is still recognizable) and a recrystallized grainstone matrix (Isern et al., 2002). Nondolomitized skeletal floatstone and grainstone lie beneath this uppermost unit (~182 to 346 mbsf), below which (~346 to 617 mbsf) occurs a thick unit of coarse crystalline dolostone. The lowermost carbonate-rich unit (~617 to 663 mbsf) also contains dolostone, though this material occurs with a significant amount of siliciclastic sediment.

Previous work suggests that meteoric diagenesis is limited at 1196 (Ehrenberg et al., 2006a). There are, however, clear physical indicators of diagenesis in the form of micritization, cementation, and dissolution at 1196 (Ehrenberg et al., 2006a), not the least of which is the presence of thick (order 200 meters) sequences of dolostone. Comparison of sediment age from biostratigraphy (Fig. 1c) to that derived from measurements of $^{87}Sr/^{86}Sr$ indicate substantial overprinting of primary $^{87}Sr/^{86}Sr$ values in both the limestones

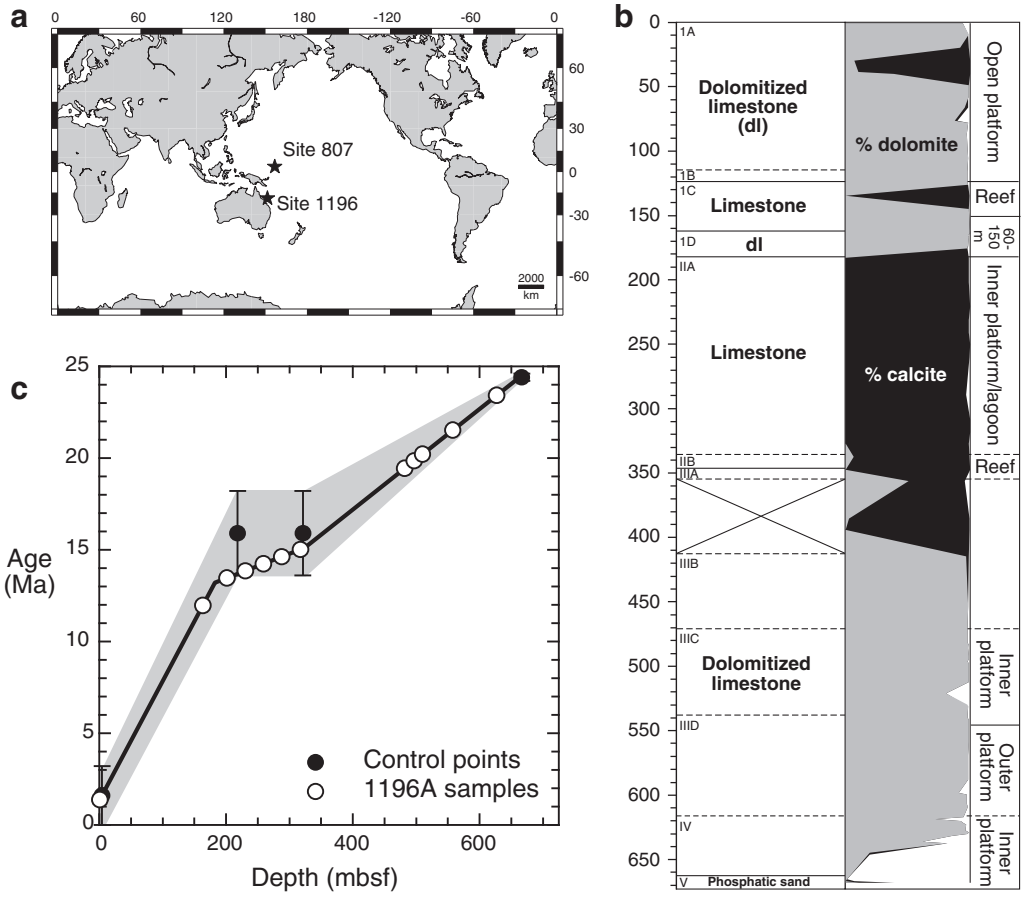

Fig. 1. (a) Site 1196A location map, with ODP Site 807A shown for reference. (b) Generalized lithologic section for Site 1196A, including XRD-based mineralogy and interpreted paleofacies (adapted from Isern et al., 2002). (c) Biostratigraphic-based age model for Site 1996A (Isern et al., 2002); closed circles (●) represent control points used to construct the age model, and the open circles (○) indicate the samples measured in the current study.

and dolostones, likely due to post-depositional diagenetic alteration (Ehrenberg et al., 2006b). The $^{87}Sr/^{86}Sr$ data seem to suggest at least two distinct diagenetic episodes. Given the uncertainty surrounding both the primary source of Sr in the diagenetic fluids and the extent of reaction, the timing of diagenesis is difficult to ascertain. If one assumes that the circulated Sr is derived primarily from seawater and that exchange between fluid and solid is complete in a relatively open system, then the major diagenetic pulse appears to occur ~10 to 15 Ma.

Such an interpretation is potentially complicated by the mixture of contemporaneous seawater with dissolved carbonate and/or basement-derived Sr, which has the potential to lower the $^{87}Sr/^{86}Sr$ of the advecting fluid considerably. It should be mentioned, however, that the slightly lower $^{87}Sr/^{86}Sr$ in 1196A limestones does not *require* a less radiogenic component (such as basalt at ~0.704) to be added. As has been observed previously, diffusion in pore fluids will smooth out the initial $^{87}Sr/^{86}Sr$ depth profile in cases where the diffusive reaction length is relatively large (Richter and Liang, 1993; Fantle and DePaolo, 2006; Fantle et al., 2010). Given the global $^{87}Sr/^{86}Sr$ curve over the last 35 Ma (McArthur and Howarth, 2004), this has the effect of lowering pore fluid $^{87}Sr/^{86}Sr$ relative to initial values.

3. GEOCHEMICAL METHODS

3.1. Calcium isotopes

Bulk carbonate samples from ODP Site 1196, Hole A were powdered in a clean agate mortar and pestle and then dissolved in dilute nitric acid (~0.5 N HNO_3: Seastar grade nitric acid and 18.2 MΩ water). The resulting solution was centrifuged and the supernatant collected for analysis. Aliquots of the supernatant were spiked with a ^{42}Ca–^{48}Ca double spike (Fantle and DePaolo, 2007) and loaded in 0.5 N HNO_3 onto single, flat, zone-refined Re filaments. After drying the sample at ~0.8 mA, ultra-pure phosphoric acid was added to the filament and dried.

Calcium isotope data were collected on the Center for Isotope Geochemistry's (CIG) Thermo Scientific Triton thermal ionization mass spectrometer at the University of California, Berkeley. A double filament assembly was used, containing two flat zone-refined Re filaments in a clean stainless steel assembly block. A typical analytical run held the evaporation filament at ~2000 mA and the ionization filament at ~3000 mA, and ran at a temperature around 1400 °C. Data were collected in four mass scans. The first collected at masses 40, 42, 43, and 44 while the second collected at masses 42, 44, 46, and 48. The third scan collected ^{39}K in the axial cup and the fourth collected at mass 49 (^{49}Ti). A typical run consisted of 200 cycles, collected in blocks of twenty. All samples were run in duplicate.

Prior to each run, a variety of potential isobaric interferences were monitored (Mg at mass 24, 25, and 26; Ti at mass 49 and 50; K at mass 39). Before the initiation of each analytical run, there was always a Mg beam (~30 to 100 mV at mass 24) on the axial Faraday cup. However, there was no indication that Mg formed a molecular ion, such as $^{24}Mg^{24}Mg^{+}$, $^{24}Mg^{25}Mg^{+}$, or $^{25}Mg^{25}Mg^{+}$. Mass scans on the secondary electron multiplier (SEM) prior to each run (at or near running intensity) generally found between 25 and 50 counts per second (cps) at mass 50 and between 0 and 100 cps at mass 49. The relative sizes of the peaks at 49 and 50 suggest that there is little Ti present and that the bulk of the 50 beam is due to ^{50}Cr (4.345%). There is typically 50–600 cps on the SEM at mass 52, which is due primarily to ^{52}Cr (83.789%). In most cases, then, the beam at mass 50 is accounted for by ^{50}Cr, and neither a molecular Mg species nor ^{50}Ti. Thus, we expect no significant isobaric interference at mass 48 from either Ti or Mg species, the effect of which is to induce artificial mass bias during double spike subtraction (Fantle and Bullen, 2009). Further, the addition of an isobaric interference at 48 would be to produce anomolously low $^{44}Ca/^{40}Ca$ ratios ($\ll 1‰$), which is opposite of the trends we interpret herein. Potassium is monitored throughout the analytical run, since isobaric interferences at mass 40 can shift the spike-subtracted ratio to lower values (Fantle and Bullen, 2009). The average ^{39}K (93.2581%) beam during a run (~1 mv) corresponds to a ^{40}K (0.0117%) beam of $\sim 2 \times 10^{-7}$ V, an inconsequential interference.

All Ca isotope data are expressed as $\delta^{44}Ca$ values relative to SRM-915a:

$$\delta^{44}Ca = \left(\frac{(^{44}Ca/^{40}Ca)_{sample}}{(^{44}Ca/^{40}Ca)_{SRM-915a}} - 1 \right) \cdot 1000 \quad (2)$$

It should be noted that the ratio reported here is the $^{44}Ca/^{40}Ca$ ratio, and not the $^{44}Ca/^{42}Ca$ ratio reported by those using MC-ICP-MS (see Fantle and Tipper, 2014 for a detailed comparison of TIMS vs. MC-ICP-MS analytical techniques and conventions). On the revised bulk Earth scale (Simon et al., 2009; Simon and DePaolo, 2010), the $\delta^{44}Ca$ of SRM-915a measured on the CIG Triton over the time period of the 1196A measurements is $-1.02 \pm 0.07‰$ (2σ; $n = 17$). Seawater measured at Berkeley has a $\delta^{44}Ca$ of 1.89‰ on the SRM-915a scale, similar to the $1.90 \pm 0.18‰$ TIMS literature average (Fantle and Tipper, 2014).

3.2. Oxygen and carbon isotopes

Both oxygen and carbon isotopic compositions were measured on aliquots of powdered bulk rocks, employing a Finnigan MAT 252 stable isotope ratio mass spectrometer equipped with a common-acid-bath automated carbonate analyzer at the Pennsylvania State University. All measured isotope ratios were corrected for ^{17}O contributions (Craig, 1957) and the measured oxygen isotope ratios corrected for fractionation during dissolution in phosphoric acid (average acid temperature during analyses = 90.83 ± 0.03 °C).

The data presented in the current study assume a kinetic fractionation factor (α, where $\alpha = R_{CO_2}/R_{carbonate}$ and $R = {}^{18}O/{}^{16}O$) for all samples of 1.008074 at 90 °C. This is similar to previously-reported values of $\alpha \approx 1.008$ for calcite at 90 °C, or 1.00989 at 25 °C (Swart et al., 1991). There is no clear consensus on the fractionation factor appropriate for dolomite, and estimates, which vary between 1.01090

and 1.01169 at 25 °C, seem to depend on the chemical composition of the dolomite to some degree (Sharma and Clayton, 1965; Land, 1980; Rosenbaum and Sheppard, 1986). Given such uncertainty, the data presented here are conservative and do not apply a dolomite-specific fractionation factor. Therefore, the reader should keep in mind that the oxygen isotopic composition of the dolostone from 1196A may be undercorrected by as much as 0.8‰ to 1‰.

All oxygen and carbon isotope data are reported in delta notation relative to the Pee Dee belemnite standard (PDB). Multiple analyses of the NBS-19 limestone standard ($n = 4$) during the analytical run resulted in $\delta^{18}O$ and $\delta^{13}C$ values of -2.19 ± 0.07‰ (2σ) and 1.97 ± 0.06‰ (2σ), compared to the accepted values of -2.20‰ and 1.95‰, respectively (Hut, 1987).

3.3. Mg isotopes and elemental compositions

Carbonate samples for Mg isotope analysis were dissolved in 0.1 N acetic acid in an ammonium acetate-acetic acid buffer (pH = 5), ultrasonicated over a 4 h period while being vented, and centrifuged. The supernatant was removed and the dissolved samples analyzed on a Thermo Scientific Element 2 inductively-coupled plasma mass spectrometer (ICP-MS) at Princeton University for major and minor elements (Mg, Ca, Sr, Al, Fe, Mn). A set of elemental standards, each containing 10 ppm Ca and varying concentrations of minor elements (Mg, Sr, Al, Fe, Mn), were used to construct calibration curves; instrumental drift was corrected using a 1 ppb Sc solution as the internal standard. The external reproducibility of the minor element ratios are better than 10%.

Sample Mg was subsequently separated from the carbonate matrix on a Dionex ICS-5000+ ion chromatograph (IC) with an AS-AP autosampler and fraction collector. Samples were separated on a CS16 analytical column with methyl-sulfonic acid as the eluent at a flow rate of 1 mL/min. The purity of a subset of separated samples was verified by ICP-MS. Final cation (Ca, Mn, Sr, Fe, Al, K)/Mg ratios within this subset were less than 0.05 (g/g). Ultrapure acids (VWR Omnitrace) and 18.2 MΩ deionized water were used in all procedural steps to ensure small procedural blanks (<10 ng Mg).

Magnesium isotopic analyses were carried out at Princeton University on a Thermo Fisher Scientific Neptune Plus MC-ICP-MS. All analyzed solutions were introduced as 150–200 ppb Mg solutions in 2% HNO_3 using a 100 µl/min PFA nebulizer and a cyclonic spray chamber under wet plasma conditions. Typical sensitivities were ~30 to 50 V ^{24}Mg per ppm Mg. Sample-standard-sample bracketing was used to correct for instrumental mass fractionation (Galy et al., 2001). Magnesium isotope ratios are reported using delta notation:

$$\delta^{n}\mathrm{Mg} = \left(\frac{(^{n}\mathrm{Mg}/^{24}\mathrm{Mg})_{\mathrm{sample}}}{(^{n}\mathrm{Mg}/^{24}\mathrm{Mg})_{\mathrm{DSM\text{-}3}}} - 1 \right) \cdot 1000 \quad (3)$$

where n is either ^{25}Mg or ^{26}Mg. Replicate measurements of the Cambridge-1 Mg isotope standard yielded $\delta^{25}Mg$ and $\delta^{26}Mg$ values of -1.34 ± 0.06‰ and -2.59 ± 0.12‰ (2σ; $n = 46$). Both measured values are indistinguishable from published values ($\delta^{25}Mg = -1.33 \pm 0.07$‰; $\delta^{26}Mg = -2.58 \pm 0.14$‰). Quantitative separation and collection of sample Mg on the IC system was verified by passing both pure Mg and synthetic dolomite (containing Mg, Ca, Na, Mn, Fe, Sr, Al, K) standards of known Mg isotopic composition through the IC. Measured $\delta^{26}Mg$ values of the Cambridge-1 and synthetic dolomite (Dol_HPS) standard passed through the IC system are -2.58 ± 0.08‰ (2σ; $n = 28$) and -0.55 ± 0.09‰ (2σ; $n = 13$), respectively, and are indistinguishable from the accepted $\delta^{26}Mg$ value for Cambridge-1 and the pure Mg standard used in Dol_HPS (-0.57 ± 0.07‰ $n = 10$). As an additional check on the sensitivity of the IC system to sample matrix, we also measured the $\delta^{26}Mg$ value of modern seawater. Measured $\delta^{26}Mg$ values of -0.77 ± 0.10‰ (2σ; $n = 5$) are indistinguishable from the published value of -0.83 ± 0.09‰ (Ling et al., 2011). Plotted in three-isotope space ($\delta^{25}Mg$ vs. $\delta^{26}Mg$) all measured samples fall on a line with a slope of 0.525 ($R^2 = 0.997$), consistent with mass-dependent fractionation of Mg isotopes.

4. RESULTS

4.1. Ca isotopic composition ($\delta^{44}Ca$)

The Ca isotopic compositions of marine limestones and dolostones from Site 1196A, which range in depth between ~58 and 627 mbsf and in depositional age between ~5 and 23 Ma, vary between 0.60‰ and 1.31‰ on the SRM-915a scale (Table 1). The highest $\delta^{44}Ca$ value occurs in dolostone near the top of the sampled section, while the lowest occurs in limestone in the middle of the section. Besides this, there is no consistent trend in $\delta^{44}Ca$ (or variance in $\delta^{44}Ca$) with age or lithology. The average limestone $\delta^{44}Ca$ is 0.97 ± 0.24‰ (1SD), which is identical within error to the average dolostone $\delta^{44}Ca$ (1.03 ± 0.15‰ 1SD).

4.2. Mg isotopic composition ($\delta^{26}Mg$)

The Mg isotopic compositions ($\delta^{26}Mg$) of marine limestones and dolostones from Site 1196A range between -2.59‰ and -3.91‰ on the DSM-3 scale. Limestones and dolostones are isotopically distinct, with averages of -3.60 ± 0.25‰ and -2.68 ± 0.07‰, respectively. There is considerably more variance in the $\delta^{26}Mg$ of limestones, and noticeable negative correlations between limestone $\delta^{26}Mg$ and both $\delta^{13}C$ and $\delta^{44}Ca$. Between the two dolostone sections, there is a slight difference (~0.1‰) between the upper and lower dolostones.

4.3. O and C isotopic compositions ($\delta^{18}O$ & $\delta^{13}C$)

The carbon isotopic compositions ($\delta^{13}C$) of Site 1196A carbonates vary between 0.86 and 2.47‰ on the PDB scale. The difference between the average measured limestone $\delta^{13}C$ (1.96 ± 0.31‰ 1SD; range: 1.51–2.26‰) and average dolostone $\delta^{13}C$ (1.68 ± 0.57‰ 1SD; range: 0.86–2.47‰) is small, with limestones average is offset to slightly higher $\delta^{13}C$ values (+0.3‰).

Table 1
ODP Site 1196A sample description, age assignments, and isotope data.

Sample[1]	Subunit	Depth mbsf	Depositional Age [2] Ma	Depositional Age Range [3] Ma	Mineralogy [4] %	$\delta^{44}Ca$ [5] ‰	2σ ‰	$\delta^{26}Mg$ [6] ‰	2σ ‰	$\delta^{18}O_{PDB}$ [7] ‰	SD ‰	$\delta^{13}C_{PDB}$ [7] ‰	SD ‰
194-1196A-													
7R-1 81-82	1A	57.7	5.1	3.2–6.7	99% dol	1.31	0.03	−2.73	0.07	4.52	0.02	2.47	0.03
18R-1 56-57	1D	163.3	12.0	10.1–14.3	100% dol (1 cm away)	0.87	0.04	−2.80	0.06	3.57	0.03	2.30	0.01
										3.36	0.02	2.11	0.02
22R-1 9-11	2A	201.2	13.5	12.5–17.0	99% cal (2 cm away)	1.13	0.09	−3.58	0.05	−0.99	0.01	2.26	0.01
25R-1 40-42	2A	230.3	13.8	13.6–18.2	99% cal	0.87	0.10	−3.55	0.05	−1.13	0.01	1.75	0.01
28R-1 9-11	2A	258.9	14.2	13.6–18.2	99% cal (1 cm away)	0.60	0.04	−3.22	0.07	−2.52	0.02	1.51	0.01
31R-1 15-17	2A	287.8	14.6	13.6–18.2	97% cal (3 cm away)	1.16	0.10	−3.91	0.05	−2.21	0.02	2.18	0.02
34R-1 64-65	2A	317.3	15.0	13.6–18.2	100% cal	1.08	0.11	−3.71	0.08	−0.23	0.03	2.04	0.02
										−0.26	0.02	2.05	0.02
51R-2 18-19	3C	481.7	19.4	18.5–21.2	99% dol (2 cm away)	0.97	0.04	−2.70	0.01	1.56	0.02	1.89	0.01
52R-5 99-100	3C	496.6	19.8	19.0–21.4	99% dol (3 cm away)	0.93	0.03	−2.66	0.04	1.18	0.02	1.65	0.01
54R-1 95-96	3C	509.9	20.2	19.4–21.7	99% dol (2 cm away)	1.07	0.03	−2.59	0.00	2.06	0.04	1.55	0.01
59R-1 72-73	3D	557.6	21.5	20.9–22.6	99% dol (1 cm away)	1.16	0.03	−2.68	0.04	3.07	0.03	0.86	0.01
										3.04	0.06	0.91	0.03
66R-2 99-100	4	626.8	23.4	23.0–23.9	99% dol (2 cm away)	0.94	0.04	−2.62	0.08	2.12	0.02	1.35	0.01

[1] Sample designated by *Leg-Hole*-Core Interval (in cm).
[2] Depositional age is assigned based on biostratigraphy (planktonic foraminifera and calcareous nannofossils), as reported by Isern et al. (2002). The time scale used is that of Berggren (1995).
[3] Age range is constrained by biostratigraphic age constraints provided by Isern et al. (2002) for Site 1196 (pp. 137–8 of that publication).
[4] Mineralogy of sample (or nearby sample; distance from measured sample noted, in cm); dol = dolomite, cal = calcite, and non-carb = non-carbonate [Table T9; Isern et al. (2002).
[5] Ca isotopic composition of bulk sample expressed relative to SRM-915a.
[6] Mg isotopic composition of bulk sample expressed relative to DSM3.
[7] Isotopic compositions determined using a common acid bath at PSU. Both oxygen and carbon isotopic compositions are expressed relative to the PBD standard. All corrections for fractionation during CO_2 evolution are made assuming calcite composition ($\alpha = 1.008074$ at 90 °C). The use of a fractionation factor for dolomite ($\alpha \approx 1.008840$ at 90 °C) would change the oxygen isotopic composition to some degree [Rosenbaum and Sheppard, 1986], but is not applied here. The NBS-19 limestone standard was run four times while analyzing the samples, with average values of $\delta^{18}O = -2.19 \pm 0.07$ (external 2σ) [reference value: −2.20‰] and $\delta^{13}C = 1.97 \pm 0.06$ (external 2σ) [reference value: 1.95‰] [Hut, 1987]. Sample replicates are noted on separate lines in the data table. 'SD' is the standard deviation of a single measurement (internal reproducibility).

Table 2
DP Site 1196A bulk sediment elemental data.

Sample	Subunit	Depth mbsf	Depositional Age Ma	Depositional Age Range Ma	Mineralogy %	Mg/Ca mol:mol	Na/(Mg + Ca) mmol:mol	Sr/(Mg + Ca) mmol:mol	K/(Mg + Ca) mmol:mol
194-1196A-									
7R-1 81-82	1A	57.7	5.1	3.2–6.7	99% dol	0.78	4.15	0.19	0.09
18R-1 56-57	1D	163.3	12.0	10.1–14.3	100% dol (1 cm away)	0.78	3.63	0.18	0.06
22R-1 9-11	2A	201.2	13.5	12.5–17.0	99% cal (2 cm away)	$3.20{\cdot}10^{-2}$	7.19	1.32	0.15
25R-1 40–42	2A	230.3	13.8	13.6–18.2	99% cal	$2.65{\cdot}10^{-2}$	7.97	1.78	0.37
28R-1 9-11	2A	258.9	14.2	13.6–18.2	99% cal (1 cm away)	$3.38{\cdot}10^{-2}$	23.64	3.49	0.44
31R-1 15-17	2A	287.8	14.6	13.6–18.2	97% cal (3 cm away)	$2.72{\cdot}10^{-2}$	8.89	0.50	0.19
34R-1 64-65	2A	317.3	15.0	13.6–18.2	100% cal	$3.60{\cdot}10^{-2}$	6.38	1.44	0.12
51R-2 18-19	3C	481.7	19.4	18.5–21.2	99% dol (2 cm away)	0.75	2.09	0.18	0.06
52R-5 99-100	3C	496.6	19.8	19.0–21.4	99% dol (3 cm away)	0.79	2.30	0.19	0.02
54R-1 95-96	3C	509.9	20.2	19.4–21.7	99% dol (2 cm away)	0.75	1.61	0.17	0.01
59R-1 72-73	3D	557.6	21.5	20.9–22.6	99% dol (1 cm away)	0.76	3.02	0.14	0.08
66R-2 99-100	4	626.8	23.4	23.0–23.9	99% dol (2 cm away)	0.87	3.66	0.10	0.19

On the other hand, the oxygen isotopic compositions ($\delta^{18}O$) of 1196A carbonates are distinctly different, even accounting for application of a dolomite-specific fractionation factor (Table 1, note 7). The average limestone $\delta^{18}O$ is $-1.22 \pm 0.94‰$ (range: $-0.23‰$ to $-2.52‰$), while the average dolostone $\delta^{18}O$ is $2.72 \pm 1.07‰$ (*range*: 1.18–4.52‰), a sizeable ~4‰ offset. The $\delta^{13}C$ and $\delta^{18}O$ data reported herein are consistent with previous studies at 1196A, which reported $\delta^{13}C$ and $\delta^{18}O$ values categorized by lithological unit (Ehrenberg et al., 2006a).

4.4. Elemental composition

Trace element to major cation ratios in Site 1196A carbonates are distinctly different between limestones and dolostones (Table 2). The average Sr/(Mg + Ca) ratio in limestones is 1.7 mmol:mol, compared to 0.2 in dolostones. The average Na/(Mg + Ca) ratio in limestones is 10.8 mmol:mol, compared to 2.9 in dolostones, while the average K/(Mg + Ca) ratio in limestones is 0.3 mmol:mol, compared to 0.1 in dolostones. As there is considerably less Mg in limestones compared to dolostones, the x/Ca ratio reported for limestones is comparable to the x/(Mg + Ca) ratio reported for dolostones.

The molar Mg/Ca ratios of limestones vary between $2.65{\cdot}10^{-2}$ and $3.60{\cdot}10^{-2}$ mol:mol, while dolostone Mg/Ca values range between 0.75 and 0.87 mol:mol (*average dolostone*: 0.78 ± 0.04 mol:mol 1SD; Table 2). The lack of stoichiometric dolomite likely indicates small calcite contributions, though it has been observed experimentally that complete recrystallization of $CaCO_3$ to dolomite can yield non-stoichiometric dolomite (Malone et al., 1996). A majority of the dolostones lie on a Mg/Ca and $\delta^{44}Ca$ trend that cannot be interpreted in terms of physical mixing between calcite and dolomite. This topic is discussed in greater detail in Section 5.2.

5. DISCUSSION

Diagenesis of marine carbonates is relevant to studies of the past for three reasons. Diagenesis can:

(1) Alter the initial solid and, thus, affect geochemical proxies used to interpret past environments,
(2) Modify the leverage of the solid in the output flux to affect the evolution of seawater isotopic composition, and
(3) Generate a distinct input flux to the ocean ("diagenetic flux"), if temporally decoupled from its initial deposition event.

The first is obviously critical, as proxy fidelity is a necessary assumption of all attempts at reconstructing the past. The corollary, however, is that Ca and Mg isotopes may prove useful tools for fingerprinting alteration in ancient rocks, once the systematics have been elucidated. The objectives of such work, then, are to avoid records that are affected by diagenetic overprinting and produce accurate interpretations of environmental changes in the geologic past.

The latter two questions have a direct bearing on the global cycles of Ca and Mg. For example, the $\delta^{44}Ca$ of the so-called "diagenetic flux" (discussed below) can range from that of seawater to any value intermediate between seawater and the $\delta^{44}Ca$ of the reacting carbonate phase. This suggests that the evolution of seawater $\delta^{44}Ca$ could

be controlled in part by diagenesis during certain periods in Earth history, and that Ca isotopes may therefore have utility for reconstructing the extent of global seafloor carbonate alteration in the past.

With these questions in mind, the subsequent discussion examines the isotopic and trace elemental consequences of diagenesis at 1196A, first setting the stage by placing the isotopic data in context. The effects of diagenesis associated with (1) limestone recrystallization and (2) dolomitization are discussed separately, and a numerical diagenetic model introduced in each case to demonstrate the feasibility of the interpretation presented. Finally, we explore the potential impact of diagenesis on the global Ca and Mg cycles via a global diagenetic flux.

5.1. Placing the isotopic compositions of shallow marine carbonates in context

Before discussing the implications of the work presented herein, we will briefly place the presented data in context. The $\delta^{44}Ca$ values of measured carbonates at 1196A are significantly higher than the mean of carbonates measured over geologic time (Fig. 2; Fantle and Tipper, 2014) and the bulk nannofossil ooze curve (Fantle and DePaolo, 2005, 2007; Fantle, 2010) (Fig. 3). A recent $\delta^{44}Ca$ compilation showed that the mean carbonate $\delta^{44}Ca$ over geologic time is ~0.6‰, or about 0.4‰ lower than the 1196A carbonates (Fantle and Tipper, 2014). This is consistent with bulk nannofossil ooze over the past 35 Ma, the average of which is ~0.7‰.

The limited number of Ca isotope measurements of modern coral vary primarily between 0.3‰ and 1‰, averaging 0.73 ± 0.18‰ (1SD; $n = 44$) for tabulated literature values (Halicz et al., 1999; Chang et al., 2004; Holmden, 2005; Böhm et al., 2006; Blattler et al., 2012; Holmden et al., 2012; Pretet et al., 2013). Chang et al. (2004) report an average coral $\delta^{44}Ca$ value of 0.63‰, while Halicz et al. (1999) report two Red Sea coral with $\delta^{44}Ca$ values ~1.2‰. These values are consistent with published average $\delta^{44}Ca$ values for modern to recent benthic foraminifera (0.68 ± 0.13‰; $n = 49$), red and green algae (0.74 ± 0.32‰; $n = 24$), and bivalves (0.78 ± 0.13; $n = 20$), which along with coral comprise the bulk of the material found at 1196A (Gussone et al., 2005; Gussone and Filipsson, 2010; Hippler et al., 2011; Blattler et al., 2012; Holmden et al., 2012).

Though not extensively sampled, the Ca isotopic compositions of ancient dolomites and dolostones have been found to vary from ~0.9‰ to values (1.8‰) that approach modern seawater (Kasemann et al., 2005; Jacobson and Holmden, 2008; Komiya et al., 2008; Tipper et al., 2008). Interestingly, Holmden (2009) calculated the $\delta^{44}Ca$ of the dolomite endmember in the Williston Basin to be 0.2‰, which is not only considerably outside the range of the few dolomites measured to date, but amongst the lowest $\delta^{44}Ca$ values reported for carbonates to date (Fantle and Tipper, 2014). This suggests, perhaps, that the Ca isotopic composition of dolomite might exhibit considerable variability, especially compared to low-Mg carbonates, that can drive the evolution of seawater over time.

Overall, the $\delta^{26}Mg$ range measured in both modern and ancient marine carbonates is quite large (Figs. 3 and 4).

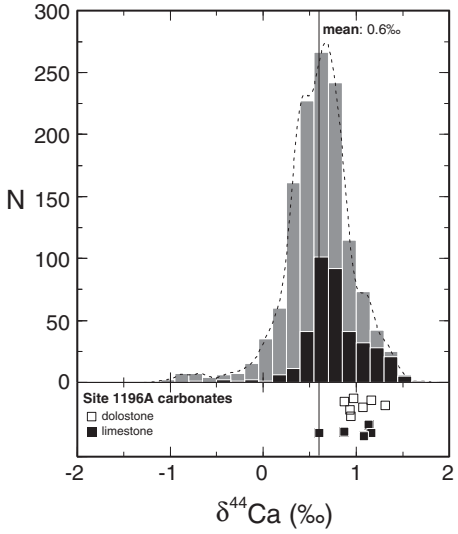

Fig. 2. Histogram of the Ca isotopic composition ($\delta^{44}Ca$, SRM-915a scale) of carbonates measured to date (compilation of tabulated literature values; Fantle and Tipper, 2014). Gray bars indicate carbonates measured over all of geologic time, while the black bars indicate Holocene carbonates.

Similar to Ca, the seawater Mg reservoir is the heaviest reservoir in the marine system (−0.8‰), and all measured carbonates to date are isotopically lighter than seawater by as much as ~5‰. The $\delta^{26}Mg$ values of 1196A limestones are comparable to other marine carbonates measured to date; the most enriched 1196A carbonate ($\delta^{26}Mg = -3.22$‰) is indistinguishable from measurements of modern coralline red algae (−3.18‰; Wombacher et al., 2011). In general, the $\delta^{26}Mg$ values of the 1196A limestones are lower than modern shallow water carbonates, though are not as low as foraminiferal carbonate ($\delta^{26}Mg$ range: −4‰ to −6‰; Fig. 4). Measured $\delta^{26}Mg$ values of 1196A dolostone are comparable to, though somewhat lower than, modern to recent authigenic dolomites formed in organic-rich marine sediments (−1.7‰ to −2.5‰; Higgins and Schrag, 2010).

With respect to carbon isotopes, both 1196A limestones and dolostones are isotopically similar to platform carbonates measured previously (Fig. 3b), at 1196A (Fig. 5) as well as the Great Bahama Bank (Malone, 2000). With respect to oxygen isotopes, there is considerably more variability in 1196A limestones compared to, for example, Great Bahama Bank periplatform carbonates deposited at similar times. There is no clear temporal trend in the oxygen isotopic composition of 1196A limestones that is comparable to that seen in benthic or platonic foraminiferal tests (e.g., Shackleton et al., 1984; Kennett, 1986; Zachos et al., 2001).

5.2. Diagenetic alteration of the proxy/output flux from the ocean

As has been discussed previously, the isotopic composition of the output flux can drive seawater isotopic composition over geologic time scales (Farkaš et al., 2007; Sime et al., 2007; Fantle, 2010; Blattler et al., 2012; Fantle and Tipper, 2014). While measurements of modern samples

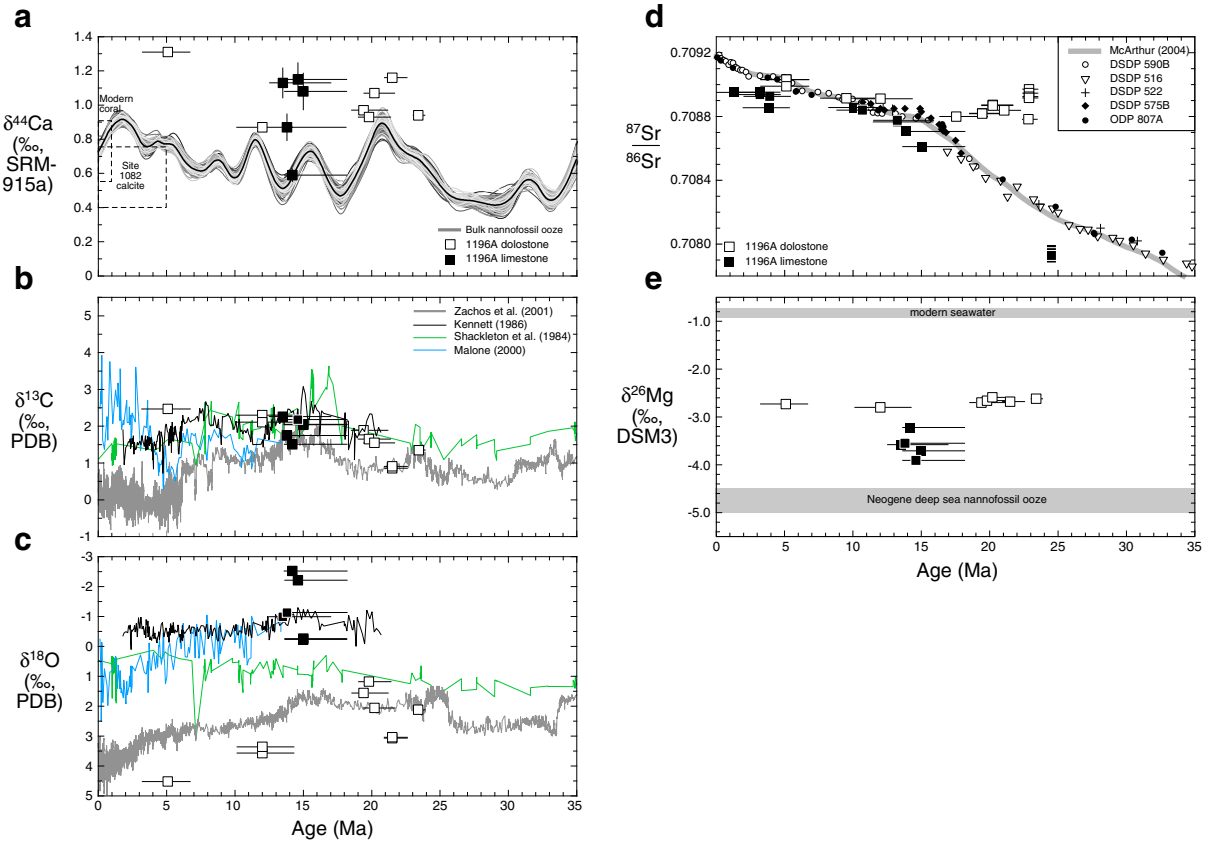

Fig. 3. (a) Ca isotopic composition ($\delta^{44}Ca$, SRM-915a scale), (b) C isotopic composition ($\delta^{13}C$, PDB scale), (a) O isotopic composition ($\delta^{18}O$, PDB scale), (d) Sr isotopic composition ($^{87}Sr/^{86}Sr$), and (e) Mg isotopic composition ($\delta^{26}Mg$, DSM-3 scale) of 1196A limestones (■) and dolostones (□) as a function of age (Ma). Shown for reference in each panel are measurements of other carbonate phases, such as: (a) the bulk nannofossil ooze curve (De La Rocha and DePaolo, 2000; Fantle and DePaolo, 2005, 2007) and Site 1082 calcite (Turchyn and DePaolo, 2011); (b–c) the benthic isotope curve (Zachos et al., 2001), an Atlantic Ocean record derived from planktonic foraminiferal tests (Shackleton et al., 1984; Kennett, 1986), and periplatform carbonates (Malone, 2000); (d) the global Sr isotope curve (McArthur and Howarth, 2004), a compilation of data from DSDP Site 590B (DePaolo, 1986; Capo and DePaolo, 1990), DSDP Site 575 (Richter and DePaolo, 1988), DSDP Site 522 (DePaolo and Ingram, 1985), DSDP Site 516 (Hess et al., 1986), and ODP Site 807A (Fantle and DePaolo, 2006) , and previously-published $^{87}Sr/^{86}Sr$ data from Site 1196A (Ehrenberg et al., 2006b); and (e) nannofossil ooze (Higgins and Schrag, 2012). All previously-published records are shown on their published time scales. The horizontal bars represent ranges in the assigned biostratigraphic ages of Site 1196A carbonates (Isern et al., 2002).

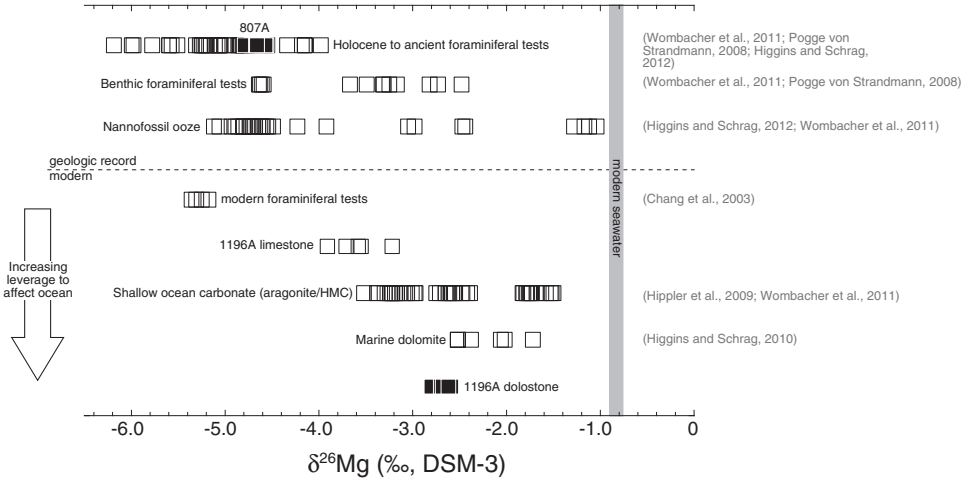

Fig. 4. The Mg isotopic composition ($\delta^{26}Mg$, DSM-3 scale) of modern and ancient carbonates.

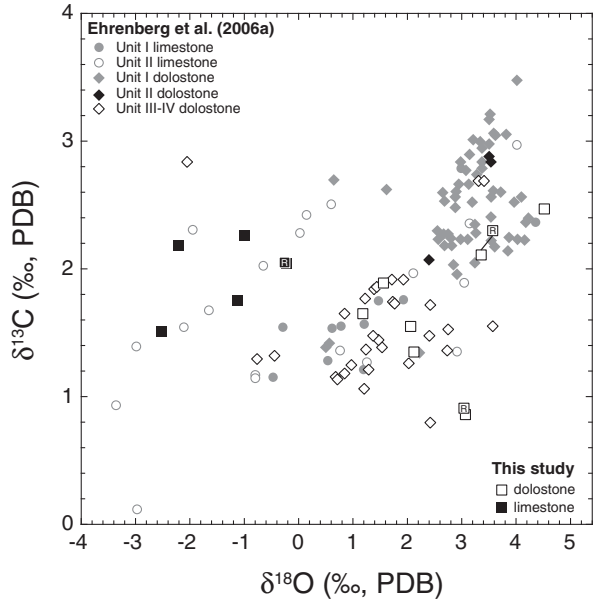

Fig. 5. The oxygen and carbon isotopic composition of carbonates from Site 1196A, including limestones (■) and dolostones (□) measured in this study and those (other symbols) reported by Ehrenberg et al. (2006a).

are critical starting points for understanding the leverage of the outputs to drive seawater evolution, it is equally important to quantify the extent to which diagenesis alters initial carbonate chemistry. This has implications for both the accurate use of geochemical proxies and the evaluation of the actual leverage of the output flux to drive seawater evolution. A precise understanding of diagenetic effects is particularly vital when considering the isotopic leverage offered by metastable forms of $CaCO_3$ (e.g., aragonite, vaterite, and ikaite) to drive seawater evolution.

Extensive diagenetic alteration is most likely to occur in shallow ocean settings, given both significant permeability and observations of fluid flow in platform carbonates (Swart et al., 1993; Ehrenberg et al., 2006a). Such settings, as compared to those dominated by diffusive transport within the pore fluid, have the greatest potential for operating as open systems in which alteration is maximized. Alteration in such settings may be especially pertinent within the global Mg cycle, as dolomite is typically formed as a diagenetic mineral in sediments, in many cases associated with advective flow regimes (Baker and Kastner, 1981; Mackenzie and Morse, 1992; Swart and Melim, 2000).

The isotopic data from Site 1196A offer insight into the geochemical effects associated with marine diagenesis over million-year time scales. The carbon and oxygen isotope data (Fig. 5), for instance, suggest that diagenesis at 1196A is not heavily influenced by meteoric fluids (Ehrenberg et al., 2006a). The samples measured in this study, as well as those reported previously from Site 1196 (Ehrenberg et al., 2006a), are within the "marine" range described by Knauth and Kennedy (2009). Thus, the interpretation below does not focus on meteoric fluids as a major component of the sedimentary system.

5.2.1. Geochemical effects associated with limestone diagenesis

The metal isotopic and trace elemental compositions of Unit II limestones are interpreted in terms of a diagenetic gradient, which may be generated by either dissolution-reprecipitation and/or net precipitation of carbonate minerals. The logic for interpreting the limestone data in terms of diagenesis, and not simply as reflecting initial isotopic compositions, are manifold. First, Unit II limestones are assumed to have originally been comprised mainly of aragonite and high Mg calcite, which are no longer present. In addition, there are clear physical indicators of micritization, cementation, and dissolution (i.e., diagenesis) in these rocks, suggestive of pervasive alteration (Ehrenberg et al., 2006a).

Second, the $\delta^{44}Ca$ of aragonite measured to date suggests a fairly low average $\delta^{44}Ca$ for a range of shallow water organisms (Gussone et al., 2005; Böhm et al., 2006; Hippler et al., 2011; Blattler et al., 2012; Holmden et al., 2012). Sclerosponge aragonite has been found to be $0.39 \pm 0.09‰$ ($n = 11$), while bivalves ($0.78 \pm 0.13‰$; $n = 20$), green algae ($0.51 \pm 0.12‰$; $n = 14$), and coral aragonite (~0.7‰) are in a similar range. While lower $\delta^{44}Ca$ values may be, in some cases, attributable to the proximity to shore (i.e., mixing between seawater and riverine/groundwater inputs that lowers fluid $\delta^{44}Ca$; cf. Holmden et al., 2012), it seems reasonable to assume that the initial $\delta^{44}Ca$ of biogenic aragonite is in the range of 0.6‰. Intriguingly, this is not only similar in a general sense to the bulk nannofossil ooze average over the past 35 Ma (Fantle and DePaolo, 2007; Fantle, 2010), but identical to bulk nannofossil ooze at the time of deposition (~14.2 Ma; Fig. 3a).

Third, the shallow limestones measured in the current study do not fall on the global $^{87}Sr/^{86}Sr$ curve but are shifted to less radiogenic isotopic compositions. This is a feature that, while not as prominent, is also noticeable in the mid-section and deeper limestones (Fig. 3d). Ehrenberg et al. (2006b) discounted detrital contamination in these rocks to explain this observation, instead suggesting that $^{87}Sr/^{86}Sr$ reflects diagenetic alteration of the original material. Thus, alteration is clearly indicated by the Sr isotope data.

Finally, there are correlated and coherent trends in isotope-isotope and trace element-isotope space that suggest alteration. The elemental trends are consistent with loss of trace elements (such as Sr and Na) in limestones (Fig. 6a), which is the expected diagenetic effect associated with the recrystallization of biogenic carbonate (e.g., Graham et al., 1982). The sample with the highest Sr/(Ca + Mg) (=3.5) and Na/(Ca + Mg) (=23.6) values is (1) at the high end of the range observed in the modern ocean for aragonite (Mitsuguchi et al., 2010), (2) close to what we infer to be the original $\delta^{44}Ca$ value (~0.6‰) for an aragonite/high Mg calcite mixture, and (3) therefore inferred to be the most pristine. For comparison, periplatform carbonates from the Great Bahama Bank, which are dominantly comprised of aragonite with minor to no dolomite, have average Sr/Ca ratios of 3.7 ± 1.7 and Na/Ca ratios of 25.6 ± 15.9 ($n = 317$; Malone, 2000). The sample identified as "most pristine" has the lowest limestone $\delta^{44}Ca$, $\delta^{13}C$, and $\delta^{18}O$ values, and the highest $\delta^{26}Mg$ value. The $\delta^{26}Mg$

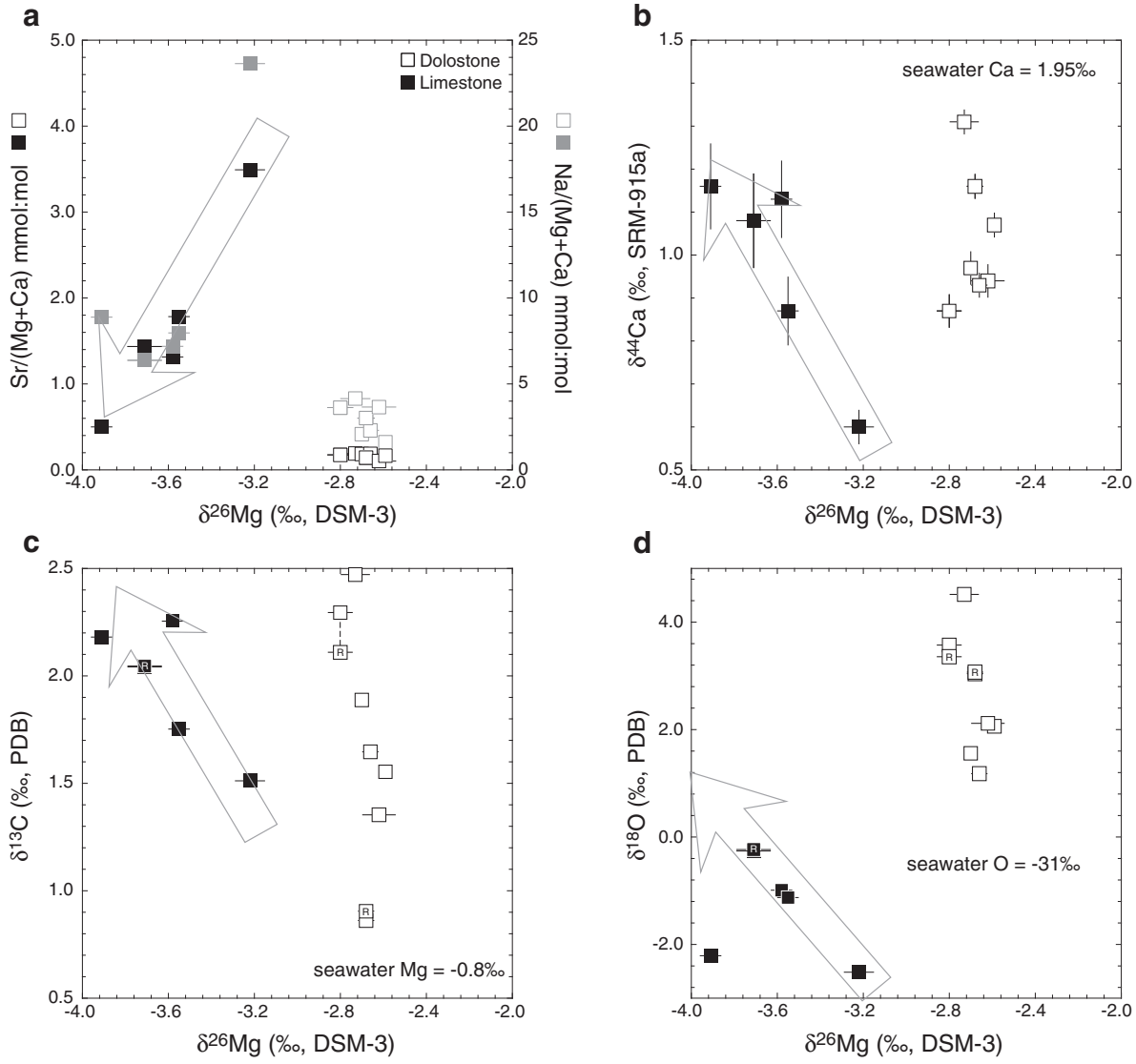

Fig. 6. (a) Trace element chemistry (Sr/(Ca + Mg) and Na/(Ca + Mg) in mmol:mol), (b) Ca isotopic composition (δ^{44}Ca, SRM-915a scale), (c) C isotopic composition (δ^{13}C, PDB scale) , and O isotopic composition (δ^{18}O, PDB scale) (d) as a function of δ^{26}Mg (DSM-3 scale) of 1196A limestones (■) and dolostones (□). In (a), the open and closed gray symbols indicate Na/(Ca + Mg) ratios, which are plotted on the secondary y-axis located on the right side of the plot. Replicate (R) analyses are plotted separately.

of this sample, in particular, is consistent with the range of shallow ocean carbonate δ^{26}Mg measured to date (excluding pelagic foraminifera), while the δ^{26}Mg values along the inferred diagenetic array are clearly outside of this range (Fig. 4).

Accordingly, we suggest that the 1196A data indicate distinct diagenetic effects on both the Ca and Mg isotopic compositions of shallow water carbonates. The overall effect of diagenesis on limestone δ^{44}Ca is to shift δ^{44}Ca to higher values (Fig. 6b). This is consistent with open system alteration in the presence of seawater, in which the advective reaction length scale is relatively large (Fantle et al., 2010). In the modern system, the average riverine δ^{44}Ca is 0.88‰ (Fantle and Tipper, 2014); assuming that the fractionation factor associated with diagenesis is close to one and that the extent of alteration is less than 100%, then diagenesis must have involved a seawater-derived component. This hypothesis is consistent with the conclusions of Ehrenberg et al. (2006a).

With regard to Mg isotopes, diagenetic recrystallization and the formation of limestone is interpreted to drive δ^{26}Mg to lighter values ($\Delta_{\text{limestone range}} \sim 0.8‰$). Assuming a seawater-like pore fluid, the relatively high fluid to solid mass ratio for Mg compared to Ca would initially suggest that δ^{26}Mg is more susceptible to diagenetic alteration than δ^{44}Ca. Yet, the slope of the interpreted δ^{44}Ca–δ^{26}Mg diagenetic trend is close to 0.7. Assuming similar initial geochemical compositions, this implies that the leverage to change δ^{26}Mg might be more similar to the leverage to alter δ^{44}Ca than otherwise assumed. This highlights the importance of accurate constraints on the diagenetic partition coefficient for Mg to the interpretation of diagenetic effects.

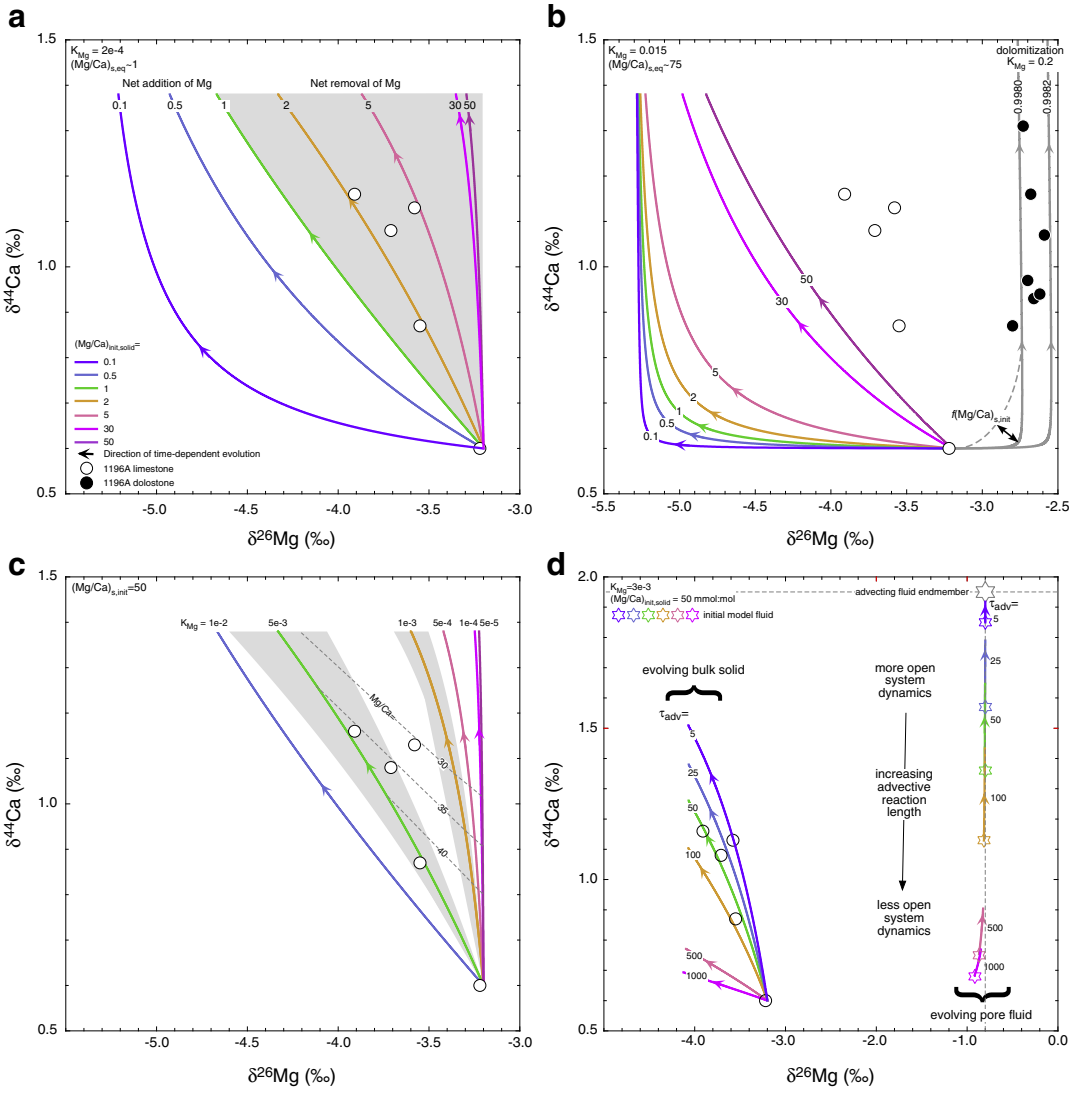

Fig. 7. Diagenetic trajectories determined using a box model simulation of carbonate recrystallization for three cases: (a) $K_{Mg} = 2 \times 10^{-4}$, (b) $K_{Mg} = 0.015$, (c) variable partition coefficient (K_{Mg}) and constant initial solid Mg/Ca (=50 mmol/mol), and (d) $K_{Mg} = 3 \times 10^{-3}$, $\alpha^{Mg}_{diag} = 0.9955$, and the advection time scale (τ_{adv}) varies between 5 and 1000. The gray shaded region in (a) indicates where net removal of Mg from the bulk solid occurs, while the gray lines in (b) indicate model "dolomitization" trends ($K_{Mg} = 0.2$; $\alpha_{precip} = 0.9980$ and 0.9982; $(Mg/Ca)_{solid,init} = 1$). The dashed lines in (c) indicate solid Mg/Ca values of 30, 35, and 40 in the evolving model solid, while the gray regions in (c) indicate the effects of varying the diagenetic fractionation factor for Mg by ±0.5‰. In all simulations, the porosity (ϕ) is constant (=0.4), the advection fluid flux is set so that the residence time of the fluid is 25 time units, the solid is modeled as a single, homogeneous reservoir, the fractionation factors associated with diagenetic reprecipitation of calcite (α_{precip}) are set to 1 for Ca and 0.9955 for Mg, the initial solid is assumed to have δ^{26}Mg and δ^{44}Ca values that are the same as the least altered sample measured at 1196A, and the advecting fluid endmember has the chemical and isotopic composition of modern seawater ($[Ca^{2+}] = 10.3$ mM, $[Mg^{2+}] = 52$ mM, $\delta^{44}Ca = 1.95‰$, and $\delta^{26}Mg = -0.8‰$). In the simulations shown in (a) and (b), the initial Mg/Ca ratio of the solid (and thus the mass balance) is varied systematically from 0.1 to 50. Each simulation is run for ⩾300,000 time units ($dt = 25$) such that isotopic equilibrium is never fully attained (i.e., for both Ca and Mg). Limestone and dolostone data from 1196A are indicated by the "○" and "●" symbols, respectively.

In addition, if one assumes a diagenetic fluid that is isotopically similar to seawater, the results imply that the equilibrium fractionation factor in this setting is significantly <1. This is consistent with *ab initio* calculations of the equilibrium fractionation factor between carbonates and aqueous Mg (Rustad et al., 2010; Schauble, 2011).

Further, it is interesting to note that $\delta^{18}O$ increases with what is inferred to be progressive diagenetic limestone alteration. Such an explanation is not consistent with diagenesis in the presence of meteoric fluid that is isotopically lighter than seawater, but is consistent with reaction in the presence of seawater at temperatures that are lower than the formation temperature (i.e., due to an increase in the fractionation factor). Such a hypothesis is consistent with Leg 194 temperature data, which are ~16 °C at the seawater–sediment interface and therefore ~8–10 °C lower than surface waters (IODP, 2014). Precipitation at lower temperatures and lower rates provide a combined ~4‰ to 5‰ of leverage

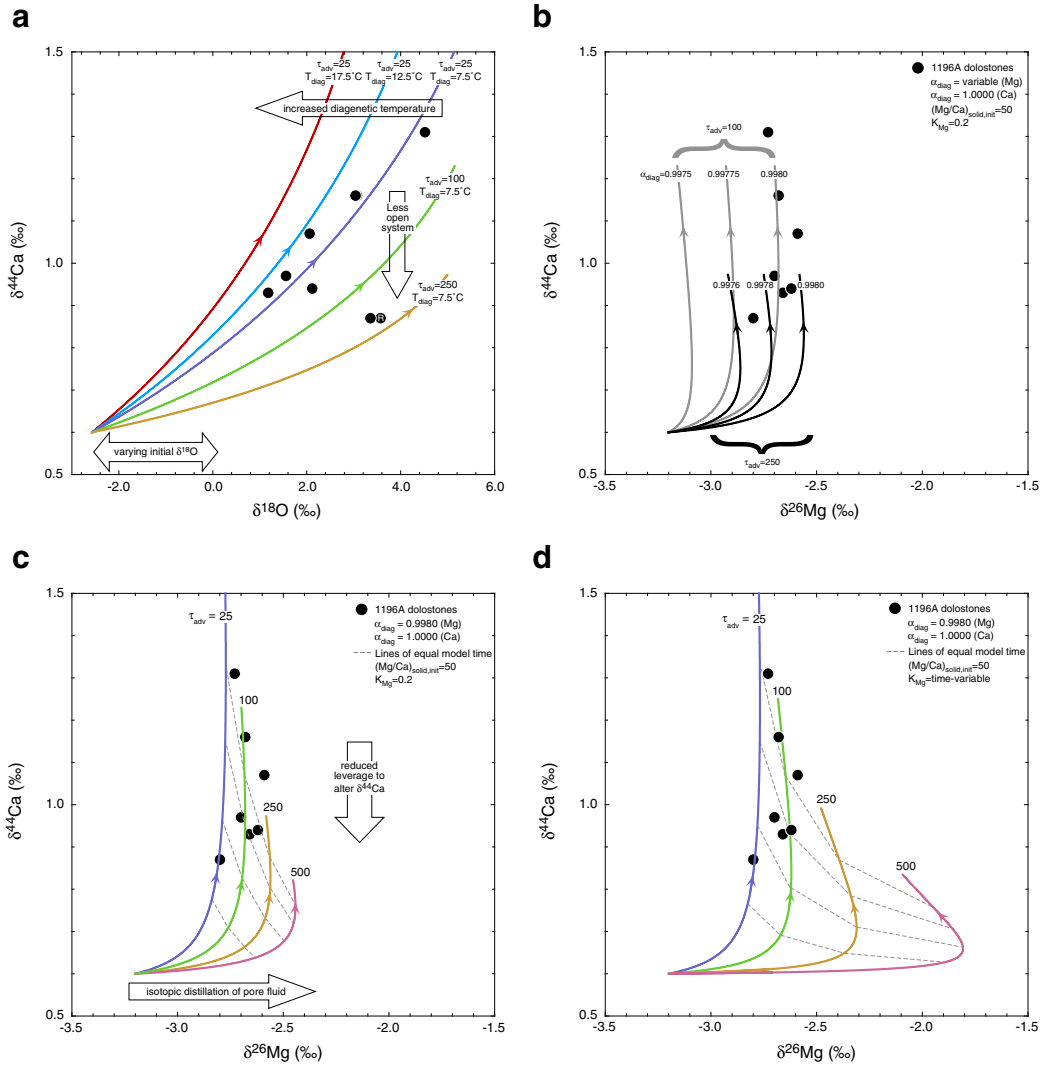

Fig. 8. Model diagenetic trajectories associated with dolomitization illustrating the evolution of a homogenous solid reservoir over time ($\phi = 0.4$). (a) Ca and O isotope trends, assuming fractionation factors for O (temperature-dependent α values associated with dolomitization; see Appendix) and Ca ($\alpha = 1.000$) and varying the advective time scale between 25 and 250. Calcium and Mg isotope trends in scenarios in which: (b) the diagenetic fractionation factor for Mg varies, (c) the advective time scale varies, and (d) K_{Mg} is constrained such that the precipitation flux has a constant molar Mg/Ca ratio of 1 (contrast with panel (c) in which K_{Mg} is constant). The dashed lines in (c) and (d) connect model solid compositions at equal model times. The initial model solid and advecting fluid endmember are compositionally identical to those utilized in Fig. 7.

to increase the $\delta^{18}O$ of carbonates relative to seawater, or more if circulating water temperatures are lower than those measured during drilling (Watkins et al., 2013). Such leverage is consistent with the $\delta^{18}O$ variability observed in the limestones (~2.3‰), as well as measurements from nearby Queensland Plateau indicating pore fluid $\delta^{18}O$ values similar to SMOW (Swart et al., 1993).

There is also a clear $\delta^{13}C$ trend in the limestones, with respect to $\delta^{44}Ca$, $\delta^{26}Mg$, and Sr/(Ca + Mg), suggesting that there is some leverage to change $\delta^{13}C$ during limestone diagenesis. In this case as well, $\delta^{13}C$ is driven to higher values (<1‰) during diagenesis. This is equally well explained by diagenesis in the presence of a seawater-like fluid at colder temperatures relative to the formation temperature. Data from the nearby Queensland Plateau suggests pore fluid $\delta^{13}C$ values between −1‰ and +1‰ on the PDB scale (Swart et al., 1993), suggesting that such a hypothesis is feasible.

5.2.2. Box model constraints on limestone diagenesis: Ca and Mg isotopes

A time-dependent recrystallization box model, described in detail in the Appendix, is employed as a first order estimate to explore the hypothesis that the limestone trends discussed above are a result of diagenesis, and to constrain the conditions under which this hypothesis is valid. At first glance, it may seem to difficult to ascribe the observed $\delta^{44}Ca$–$\delta^{26}Mg$ trend to diagenesis. Given the relatively high fluid to solid mass ratio of Mg compared to Ca, it is easy to imagine that Mg is substantially more susceptible to

alteration than Ca (Eq. (1)), which is not what the data appear to indicate.

To explore the feasibility of this hypothesis, endmember scenarios are explored in which the advection regime is held constant (advective time scale, $\tau_{adv} = 25$ time units). The diagenetic fractionation factors ($\alpha^{Ca}_{diag} = 1; \alpha^{Mg}_{diag} = 0.9955$), and initial solid $\delta^{44}Ca$ (+0.6‰) and $\delta^{26}Mg$ (−3.2‰) values are assumed, while the relative mass transfer of Mg between fluid and solid is varied (Fig. 7). The advective time scale is chosen to be sufficiently small so that the $\delta^{26}Mg$ of coexisting pore fluid is isotopically similar to modern seawater, though modified to lower $\delta^{44}Ca$ values by the dissolution of the bulk solid (Fig. 7). Because seawater $\delta^{44}Ca$ and $\delta^{26}Mg$ are both significantly higher than the respective carbonate reservoirs in the marine system, this approach ensures considerable isotopic leverage to alter the solid.

The simulations clearly demonstrate that the trend in limestone $\delta^{44}Ca$ and $\delta^{26}Mg$ (Fig. 6b) can be explained by diagenetic recrystallization (Fig. 7), yet highlight that the relative mass balance of the solid phase is a critical factor. As expected, highly non-linear trends in $\delta^{44}Ca$–$\delta^{26}Mg$ space result in cases where the Mg in the solid is well out of elemental equilibrium with the fluid. However, in cases where the solid is close to elemental equilibrium, the $\delta^{44}Ca$ and $\delta^{26}Mg$ alteration trends are considerably more linear, with slopes approaching those of the 1196A limestones (Fig. 8). The simulations also illustrate that while the leverage to alter Mg isotopes is maximized over a range of advective time scales, the leverage to alter Ca isotopes is likely never maximized. This is because the advecting endmember is easily influenced by carbonate dissolution and its $\delta^{44}Ca$ lowered (see Section 5.3).

The simulations suggest that the K_{Mg} value associated with carbonate diagenesis at 1196A is likely substantially lower than 0.015 (Fig. 7b), the minimum value observed in laboratory experiments (e.g., Oomori et al., 1987), and instead may be closer to ~1 to $5{\cdot}10^{-3}$ (Fig. 7c). This is strikingly similar to the empirical K_{Mg} value applied by Fantle and DePaolo (2006) in modeling recrystallization of nannofossil ooze at ODP Site 807A (order$\sim 1{\cdot}10^{-3}$), and also similar to the value recently constrained by Higgins and Schrag (2012), also at 807A (order$\sim 2{\cdot}10^{-3}$). Our value is also consistent with the K_{Mg} (associated with carbonate recrystallization) constrained by Baker et al. (1982) at DSDP Site 305 ($\sim 8.1{\cdot}10^{-4}$). Such a value, which is ~15 to 60 times lower than those reported in low temperature laboratory studies (e.g., Katz, 1973; Oomori et al., 1987), indicates not only a strong rate dependence for K_{Mg} but also that K_{Mg} values constrained in experimental settings are not necessarily applicable to diagenesis. Using studies of natural systems to constrain such parameters is, therefore, critical.

While unavoidable, uncertainty surrounding the advective regime is important to consider when interpreting the 1196A data in light of the model results. Decreasing the advection flux relative to the recrystallization rate decreases the extent to which the solid is out of isotopic equilibrium, reducing the leverage to alter the solid (Fig. 7d). Increasing the advection flux has the opposite effect. Yet over an approximate two orders of magnitude range of advective time scales (~1 to 100), the overall trajectories in $\delta^{44}Ca$–$\delta^{26}Mg$ space are similar. Thus, while the advective regime is critical for the purposes of either (1) interpreting the extent to which a given material is altered over a given time interval or (2) utilizing a diagenetic effect to constrain diagenetic time scales, neither are goals of the present work and the uncertainty associated with the advective time scale is acceptable.

While the value of the Ca isotopic fractionation factor is uncertain, constraints on the fractionation factor associated with recrystallization in bulk nannofossil ooze and experimental work on fractionation during calcite precipitation both suggest a value close to 1 is reasonable (Fantle and DePaolo, 2007; Tang et al., 2008, 2012). This, to a certain extent, is a conclusion that is demanded by the 1196A data. The data cannot be explained at all if the fractionation factor associated with recrystallization is substantially less than 1; in fact, simulations support a fractionation factor >0.9996 in a completely open system in order to explain the limestone data. In addition, as we are not attempting to interpret extents of recrystallization in this modeling exercise, this assumption is not overly critical to the conclusions made here as long as the diagenetic fractionation factor is significantly closer to one than that associated with carbonate formation in the water column. The assumed value of the Mg isotopic fractionation factor associated with diagenesis is based on a variety of work, including *ab initio* calculations of the equilibrium fractionation factor between aqueous Mg and calcite and studies of recrystallization in the natural system (Higgins and Schrag, 2010; Rustad et al., 2010; Schauble, 2011). Again, this assumption is not overly critical to the conclusions made herein, though it will affect the trajectories to some extent.

Furthermore, given modern seawater chemistry (Mg/Ca = 5 mol/mol), the fluid to solid mass ratio of Mg is far greater than Ca in the sedimentary system. While seawater chemistry may evolve over long time scales, it seems unlikely that Ca and Mg fluid to solid mass ratios will ever be comparable. Thus, as advection fluid fluxes decrease, it seems safe to assume that the leverage to alter Ca decreases well before Mg (Fig. 7d), which is reflected in the slopes of the solid alteration curves shown in Fig. 7d.

5.2.3. Geochemical effects associated with dolomitization

At Site 1196A, dolomitization of platform carbonates has occurred in the upper 180 m (Unit I) as well as at depth (~350–650 mbsf; Units III and IV), in what have been interpreted to be originally open and inner platform facies (Fig. 1b). It has been hypothesized previously that Site 1196A Unit I dolostones formed at low temperature from seawater while Unit III and IV dolostones formed at slightly higher temperatures, also in contact with a seawater-like fluid (Ehrenberg et al., 2006a). Further, previously-published Sr isotope data indicate that Unit III and IV dolostones are substantially shifted to more radiogenic $^{87}Sr/^{86}Sr$ values relative to their inferred initial values, strongly suggesting interaction with a younger seawater fluid (Fig. 3d; Ehrenberg et al., 2006b).

As with the limestones, dolostone $\delta^{44}Ca$, $\delta^{13}C$, and $\delta^{18}O$ vary markedly at 1196A. By contrast, the $\delta^{26}Mg$ and trace element ratios of the dolostones are relatively invariant.

This can be interpreted in terms of mass balance, and the difference between diagenetic effects on major and trace elements. Clearly, the addition of Mg to marine carbonates during dolomitization completely overwrites the initial Mg isotopic composition. If it is assumed that dolostone δ^{26}Mg values reflect equilibration with a fluid that has a δ^{26}Mg value close to −0.8‰ (i.e., that of modern seawater), a fractionation factor associated with dolomitization of approximately −2‰ is implied.

Similar to the variably altered limestones, the isotopic compositions of the major elements in dolostones from 1196A appear to trace out diagenetic trends. As δ^{44}Ca increases towards the maximum dolostone value, δ^{18}O increases by ~3.3‰ and δ^{13}C decreases towards 0‰, suggesting dolomitization of limestone with initial δ^{44}Ca <0.6‰, δ^{13}C >2‰, and δ^{18}O <1‰. Such initial oxygen and carbon isotopic compositions agree with reported values for shallow water organisms (e.g., Milliman, 1974; Anderson and Arthur, 1983).

The dolomite δ^{18}O trend is consistent with reaction in the presence of seawater ($\delta^{18}O_{sw} \sim -31‰$ on the PDB scale), and a fractionation factor that is larger than that associated with initial carbonate formation. There is both experimental and theoretical support for a substantial dolomite-water fractionation factor (>32‰) at temperatures less than 25 °C, which is at least ~4‰ to 5‰ greater than the corresponding calcite-water fractionation factor (Northrop and Clayton, 1966; Clayton et al., 1968; Fritz and Smith, 1970; Sheppard and Schwarcz, 1970; Rosenbaum and Sheppard, 1986; Schmidt et al., 2005; Schauble et al., 2006; Chacko and Deines, 2008; Horita, 2014). The observed trend at 1996A, therefore, is consistent with what is known regarding oxygen isotopic fractionation associated with dolomite formation.

The feasibility of such a mechanism is illustrated in Fig. 8a, which applies the numerical box model to oxygen, in addition to Mg and Ca, isotopes. The model approximates the δ^{44}Ca–δ^{18}O trend that would result if an initial solid with $\delta^{44}Ca = 0.60‰$ and $\delta^{18}O = -2.57‰$ equilibrates at a range of diagenetic temperatures (7.5–17.5 °C) and varying extents of open system behavior. The fractionation factor associated with dolomitization is estimated from the equation in Horita (2014), which is described in the Appendix (Eq. (A11)). The model makes it clear that the oxygen isotopic data can also be explained by diagenesis, and further suggests that offsets from the open system trend is likely a result of increasingly closed system behavior, and not temperature. This is logical, considering that the leverage to alter Ca will decrease before that to alter oxygen, given their relative fluid to solid mass ratios.

Such an interpretation suggests that the dolostone at 163.3 mbsf formed either in a setting that was considerably more closed (by factor of ~4 to 10) than those at other depths, or from a material with a markedly higher initial δ^{18}O. The value chosen for the initial δ^{18}O is decidedly uncertain and may be higher by about 2–3‰ than the value chosen. Regardless, the former hypothesis not only explains the oxygen isotope data, but also accounts for the rather low δ^{44}Ca value at 163.3 mbsf (via decreased leverage to alter Ca isotopes with increasing advective time scale). In order for this interpretation to be consistent with the Mg isotope datum at this depth, the fractionation factor associated with dolomitization would have to be slightly lower than 0.9980 (i.e., ~0.9977; Fig. 8b), which is considered to be within the uncertainty of the fractionation factor estimate.

Decreasing δ^{13}C with progressive alteration can be explained by considering that the equilibrium fractionation factor for dolomite relative to calcite is on the order of about +2.5‰ ($T < 25$ °C), while dolomite at low temperatures is isotopically heavier (~>10‰) relative to CO_2 (Sheppard and Schwarcz, 1970; Deines, 2004; Schauble et al., 2006; Horita, 2014). Thus, the 1196A data are consistent with dolomitization in the presence of a fluid carbonate reservoir that has a δ^{13}C value that is isotopically lighter than seawater. In the nearby Queensland Plateau (ODP Leg 133), isotopically light fluids are observed at the top of the sections at Sites 819–822 (Swart et al., 1993), likely related to sulfate reduction and organic matter remineralization in the sedimentary column (Baker and Kastner, 1981). We suggest that the diagenetic trend in dolostone δ^{13}C, therefore, reflects the formation of dolomite in equilibrium with a fluid that has a δ^{13}C value less than −10‰ and a dolomite-CO_2 fractionation factor on the order of 10‰.

One exception to the diagenetic dolostone trend in δ^{13}C noted above is the uppermost dolostone sample at 57.7 mbsf, which lies on the previously-described dolomite δ^{18}O-, δ^{44}Ca-, and trace element- δ^{26}Mg trends. In these respects, the shallowest dolostone isotopically and geochemically resembles limestone altered to dolomite, indicating considerable re-equilibration with seawater. The δ^{13}C of this dolostone (2.5‰), however, does not follow the same diagenetic trajectory towards 0‰ with increasing extent of alteration as the other dolostones. This is difficult to explain, as neither the carbon nor oxygen isotopic compositions of this Unit I dolostone are anomolous compared to the more extensive dataset published previously (Ehrenberg et al., 2006a). Previously measured dolostones from 1196A have δ^{13}C values as high as 3.3‰, while the δ^{18}O of the 57.7 mbsf dolostone is at the isotopically heavy limit of measurements reported previously (Ehrenberg et al., 2006a).

It has been hypothesized that some Unit I and II dolostones underwent extensive early cementation relative to other units (Ehrenberg et al., 2006b). The data imply, then, that there was leverage to change Ca, Mg, and oxygen (but not carbon) isotopic compositions during shallow dolomitization. This further suggests that the leverage to change δ^{13}C varies within the section. Such a hypothesis is supported by the presence of considerable δ^{13}C gradients in the upper 100 m of Queensland Plateau pore fluids (Swart et al., 1993). If it is true that the leverage to alter δ^{13}C derives primarily from isotopically light fluids associated with the oxidation of organic matter, then the 57.7 mbsf datum suggests that this leverage may not always be expressed. This may occur for a variety of reasons, including relatively low rates of oxidation and/or comparatively fast fluid advection (i.e., large advective reaction length scale).

Finally, while we cannot dismiss the hypothesis that the initial $\delta^{44}Ca$ of the sample at 57.7 mbsf was considerably higher than the samples farther downsection, resulting in considerably lower leverage to alter $\delta^{44}Ca$, we suggest such a scenario is unlikely. Two lines of reasoning support this contention: one, given that constraints on the microfacies biogenic components in the upper 350 m of 1196A indicate that red algae are a much more significant component at depths shallower than ~175 mbsf than at depths greater than 175 mbsf (Conesa et al., 2005), the biogenic components comprising the dolostone sample at ~163.3 mbsf should be almost identical to those at 57.7 mbsf. Yet, the Ca isotopic composition of the two are vastly different (0.87 vs. 1.31‰, respectively). We do note that there is a degree of uncertainty surrounding this assumption given that modern red algae have a sizeable range of $\delta^{44}Ca$ values (1.05 ± 0.23‰ 1SD) and are considerably undersampled ($n = 10$). Two, there are no trends in the sensitive trace element data that suggest a significant proportion of the original geochemical signal is present in the 57.7 mbsf dolostone. In addition, the oxygen isotopic composition of the 57.7 mbsf dolostone clearly lies on the alteration trend, suggesting enough leverage to affect major elements. We therefore conclude that the aberrant $\delta^{13}C$ is a function of isotopic gradients, or little leverage to alter $\delta^{13}C$, at the top of the section.

5.2.4. Box model constraints on dolomitization: Ca and Mg isotopes

In $\delta^{44}Ca$–$\delta^{26}Mg$ space, the measured trend at 1196A is consistent with varying extents of isotopic equilibration during dolomitization. During dolomitization, it is expected that the $\delta^{26}Mg$ of relatively low-Mg carbonates will be rapidly overwritten, while $\delta^{44}Ca$ will change more slowly. This is precisely what is observed in the box model (Fig. 7b and 8), in which Ca mass loss from the solid is exactly balanced by Mg gain (Appendix, Eq. (A10)).

As discussed in Section 5.2.2, the diagenetic fractionation factor for Ca is assumed to be one in the models. Limited experimental data suggest that microbially-mediated dolomite is isotopically light (Krause et al., 2012); however, given the well-known experimental dependence of fractionation factor on precipitation rate for $CaCO_3$ phases, it is not clear if such experiments are applicable to diagenetic reactions in natural systems. In addition, theoretical calculations suggest that, at equilibrium, dolomite should be isotopically lighter than coexisting calcite (Rustad et al., 2010). Again, it is difficult to know how applicable such studies are to natural systems, which may deviate from *ab initio* calculations due to precipitation mechanism, the formation of metastable or non-stoichiometric phases, the effects of impurities in the structure, kinetic isotope effects, etc. Accordingly, we acknowledge that a diagenetic fractionation factor for Ca less than one is plausible, and that this will compress (to a limited extent) the vertical dimensions of the trajectories presented in Fig. 8.

Given the assumptions of the model, most importantly the extent to which the system is open, the dolostone data are consistent with a diagenetic fractionation factor (α^{Mg}_{diag}) of 0.9980. The constraint on the fractionation factor is broadly consistent with previous estimates of the fractionation factor associated with dolomitization based on measurements from authigenic dolomites formed in organic-rich marine sediments (Higgins and Schrag, 2010). The $\delta^{26}Mg$ values of organogenic dolomites are substantially enriched ($\delta^{26}Mg$: −1.7‰ to −2.5‰) compared to the measured $\delta^{26}Mg$ values at Site 1196A, suggesting a difference in isotopic systematics.

Although rate-dependent fractionation cannot be discounted, one possible explanation for this difference is the relative importance of advection and diffusion (and/or the advective reaction length scale) in supplying Mg to the site of dolomite precipitation. In cases where Mg is predominately supplied by diffusion (i.e., organogenic dolomites in deep-sea marine sediments), variations in the rate of Mg supply relative to the rate of dolomite formation may result in conditions in the pore fluid-sediment system that resemble a more closed system. Such an explanation predicts that diffusively-controlled organogenic dolomites have a large range of $\delta^{26}Mg$ values, with the lowest $\delta^{26}Mg$ values corresponding to more open system conditions and the highest $\delta^{26}Mg$ values corresponding to more closed system conditions. By contrast, in systems where Mg is supplied largely by advection, such as shallow water carbonate platforms like Site 1196A, more homogeneous $\delta^{26}Mg$ values would be expected due to open system conditions.

An example of the relationship between dolomite $\delta^{44}Ca$ and $\delta^{26}Mg$ values and the extent to which the sedimentary system is open is shown in Fig. 8. Given the assumptions and simplifications made in the model, there are three observations to note. First, isotopic distillation of the pore fluid impacts the $\delta^{26}Mg$ of the solid markedly as the advective time scale varies by a factor of twenty to forty (Fig. 8c and d). The time-dependent distillation trend early in the evolution of the system also depends on the initial Mg/Ca of the solid and the K_{Mg} value (Figs. 7b and 8d).

Second, the 1196A dolostone data appear to be grouped in $\delta^{44}Ca$–$\delta^{26}Mg$ space along lines of equal time (Fig. 8d), yet the data in each group are not simply related to each other by proximity in the sedimentary column. Following this line of reasoning, dolostones at 57.7, 557.6, and 509.9 mbsf could be interpreted as experiencing the longest duration of diagenesis. The shallowest sample is consistent with formation in an open system, while deeper samples suggest formation in increasingly closed systems. Dolostones at 481.7, 496.6, and 626.8 mbsf are grouped together, suggesting a similar advective regime and a similar alteration time scale. This hypothesis might also explain the differences in the $^{87}Sr/^{86}Sr$ observed in dolostones at 1196A. The dolostone at ~58 mbsf, which has the highest $^{87}Sr/^{86}Sr$ value (0.709032) that is most similar to the assumed advective fluid, is assumed to have formed in a fairly open system and undergone extensive alteration. By contrast, the lowest dolostone $^{87}Sr/^{86}Sr$ measured has a value of 0.708783 (~605 mbsf), at which depth the system appears more closed (and thus less reflective of the advective endmember) and the extent of alteration is consequently lower.

Third, the extent to which the initial solid $\delta^{44}Ca$ is altered *over a given time period* is substantially diminished as the advective time scale increases. In the rock record, this

decrease in $\delta^{44}Ca$ variability will correspond with considerable $\delta^{26}Mg$ variability (about 1‰) at low extents of alteration. Thus, diagenetic dolomite trends in the rock record can potentially provide information not only on the extent of diagenesis but also, given constraints on the fractionation factor, on the advective regime.

Interestingly, increasing the advective time scale can create pore fluids in diagenetic systems that are considerably heavier than seawater (e.g., ~ pore fluid $\delta^{26}Mg$ values of 1.1‰ for $\tau_{adv} = 2000$, $K_{Mg} = 0.2$). This is a potential mechanism for creating authigenic carbonates along the flow path that are isotopically heavier than seawater or that form a distinct input flux to the ocean that can alter seawater isotopic composition (see Section 5.3).

5.2.5. Consideration of physical mixing

It is important to note that physical mixing is a possible explanation for at least some of the data trends observed. In particular, a subset of the dolostones (at 163.3, 496.6, and 626.7 mbsf) lie along a poorly defined line ($R^2 = 0.5$) in $\delta^{44}Ca$–Mg/Ca space that could be interpreted as reflecting physical mixing between a low Mg endmember and stoichiometric dolomite. For comparison, no similar trend is noted in the limestone data. In the case of the dolostone subset, the limestone endmember is estimated to have a $\delta^{44}Ca$ of ~0.5‰ and the stoichiometric dolomite endmember a $\delta^{44}Ca$ of 1‰, significantly lower than other dolostones in the dataset. This suggests that simple mixing between an endmember dolomite and primary calcite does not explain all the data. Furthermore, the same subset of dolostones does not follow the expected mixing trends in $\delta^{44}Ca$–$\delta^{18}O$, $\delta^{44}Ca$–$\delta^{13}C$, or $\delta^{44}Ca$-trace element ratio space. In the case of oxygen and carbon isotopes, for example, a mixing analysis would suggest a rather unreasonable calcite endmember on the order of ~14‰ ($\delta^{18}O$) and ~7.4‰ ($\delta^{13}C$). Finally, with respect to Mg, mass balance constrains the calcite to dolomite mass ratio in potential mixtures to be <0.18 g/g in all samples measured. Given the low Mg concentrations of the limestones at 1196A, >95% of the Mg must therefore be derived from the dolostones, obviating the issue for Mg. The data may be technically compatible with an endmember mixing hypothesis that considers physical mixtures of three components: primary carbonate, diagenetic limestone, and diagenetic dolomite. However, it is not clear that such an approach is distinct from the preferred box model approach. It could be argued that the two are conceptually similar, in that both ultimately describe the geochemical evolution of a volume of sediment from an initial to a final state via dissolution and reprecipitation. While mixing might describe the effect of replacing volume fractions of sediment by an invariant endmember, the diagenetic model attempts a holistic approach. In other words, the diagenetic model considers the entire system, approximating the mechanism of reaction in a simple manner, while the mixing model does not deal with mechanism at all and simply assumes the presence of distinct endmembers in various proportions whose creation is not genetically tied to any process. Such an approach may prove inexact, because of time-dependent evolution of the pore fluid that alters the composition of diagenetic minerals. In the end, it is perhaps useful to consider the diagenetic model presented herein and a physical mixing model as comparable, with the diagenetic model preferred here due to the constraints offered on the temporal evolution of the system.

5.3. Implications for the global Ca and Mg cycles

It has previously been observed that the non-radiogenic silicate rocks have an average $\delta^{44}Ca$ value of 0.94‰, which is similar to the average riverine $\delta^{44}Ca$ (0.88‰) but significantly higher than the average $\delta^{44}Ca$ of carbonates (0.61‰; (Fantle and Tipper, 2014). Over the past 35 Ma, the bulk nannofossil ooze average is also lower than rivers ($\delta^{44}Ca$ ~0.7‰; (Fantle and DePaolo, 2005, 2007; Fantle, 2010). In the global Ca cycle, the primary input to the ocean is rivers, and the $\delta^{44}Ca$ of rivers is not the same as that of the primary output (carbonate). The simple inference, then, is that the Ca cycle is not in steady state.

Following this logic, the question that immediately arises is whether or not there is a sizeable component of the Ca cycle that has not been adequately measured and makes up this gap. Holmden et al.'s (2012) suggestion of a significant and isotopically distinct submarine groundwater discharge (SGD) is certainly viable, though it is unclear what the isotopic leverage is in this input to alter the $\delta^{44}Ca$ of the input flux. The local Florida Bay SGD input constrained by Holmden et al. (2012) is isotopically identical to global rivers, thus offering no distinct leverage to alter the $\delta^{44}Ca$ of the input flux to the ocean. The calculated global SGD input assuming steady state is the same as the global carbonate average, and therefore provides significant leverage to alter input $\delta^{44}Ca$. While completely plausible, it has not been confirmed by field measurements that such a SGD flux exists. Alternatively, we propose that such a flux may be supplemented by a diagenetic carbonate flux generated in the marine environment.

This hypothesis assumes that marine diagenesis substantially shifts the $\delta^{44}Ca$ of the output flux to higher values than those imparted during initial precipitation. The data from 1196A, which suggest $\delta^{44}Ca$ values of altered carbonates on the high end of the global carbonate distribution (1.01 ± 0.11‰ 2σ), support this hypothesis. The effect of this mechanism is to alter the $\delta^{44}Ca$ of the coexisting pore fluid, which may then be input back into the ocean and affect the evolution of seawater $\delta^{44}Ca$. Such a mechanism is likely most important in sedimentary sections that experience relatively rapid, externally forced advection, as in shallow water carbonates or perhaps thin, permeable <350 meter-thick nannofossil ooze sections.

If the diagenetic effect can be constrained, this information could prove useful for constraining the proportion of Ca removed from the marine system by a given mode at steady state. An example calculation, assuming an input flux to the ocean of 0.88‰ and endmember $\delta^{44}Ca$ values for the output fluxes of 0.7 (bulk ooze output) and 1.0‰ (shallow carbonate output), suggests that steady state could be attained in the marine Ca cycle if the relative mass fluxes of Ca in nannofossil ooze and platform carbonates are ~30% and 70%, respectively.

Depending on the time scale over which diagenesis operates relative to deposition, diagenesis can impact the global Ca cycle in two main ways. As alluded to above, one can consider the output flux to have been altered instantaneously if diagenesis operates on a time scale similar to the residence time of Ca in the ocean. In this case, diagenesis can be thought of as altering the global fractionation factor ($\Delta^{\text{global}}_{\text{output}}$) associated with removal of Ca from the ocean. Mechanistically, alteration of the output flux can occur via a net addition of Ca to the output flux by either net dissolution of authigenic carbonate and/or recrystallization. Alternately, if diagenetic alteration occurs over time scales substantially longer than the oceanic residence time of Ca, then the effect of diagenesis on the global Ca cycle is to create a distinct input flux to the ocean that can impact the isotopic composition of the ocean.

To place this discussion in context, consider that the steady state evolution of seawater δ^{44}Ca or δ^{26}Mg is controlled by the isotopic compositions of both the input (i.e., riverine, groundwater, and hydrothermal fluxes) and output fluxes (i.e., the global fractionation factor) (e.g., De La Rocha and DePaolo, 2000; Fantle and Tipper, 2014):

$$\delta_{\text{ocean}} = \sum_{\text{inputs,i}} \delta_i X_i - \Delta^{\text{global}}_{\text{output}} \quad (4)$$

where X_i is the mole fraction of Ca or Mg in the i^{th} input flux. Diagenesis has the potential, therefore, to affect either term on the right-hand side of Eq. (4). Take, for example, the case of Ca: assuming a diagenetic fractionation factor ($\alpha^{\text{Ca}}_{\text{diag}}$) close to 1, the effect of diagenesis in the global Ca cycle is always to move the output flux closer to the relevant fluid δ value. In most cases, we assume that fluid is seawater-like (i.e., $\delta^{44}\text{Ca} = 1.95‰$), but the validity of this assumption depends on the advective regime (i.e., the advective reaction length scale; Fig. 7d). In the Ca cycle, diagenesis generally acts to moderate the evolution of seawater isotopic composition by reducing the leverage of the output flux to drive changes in δ^{44}Ca, effectively acting as a feedback to buffer the amplitude of temporal variability.

In situations where the global fractionation factor ($\Delta^{\text{global}}_{\text{output}}$) changes in time, however, both positive and negative feedbacks are possible. Again, consider the Ca cycle scenario in which the global fractionation factor becomes more negative, preferentially removing more isotopically light Ca and driving ocean δ^{44}Ca to higher values (Sime et al., 2007; Fantle, 2010; Fantle and Tipper, 2014). In this case, diagenesis will mitigate the magnitude of the change in oceanic δ^{44}Ca by decreasing the global fractionation factor, if it operates within ~500 ka following deposition. On the other hand, if the global fractionation factor becomes more positive over time (e.g., from −1.5‰ to −0.5‰), then diagenesis can enhance the magnitude of the change by driving the output flux closer to pore fluid (and ostensible seawater-like) δ values.

Diagenesis can also generate a distinct input flux to the ocean, thereby affecting the first term in Eq. (4). Such a role is only relevant in cases where: (1) diagenesis acts over time scales greater than the response time of Ca or Mg in the global ocean subsequent to deposition, and (2) pore fluid Ca or Mg is input back into the ocean. The second point is not trivial, and should be kept in mind when considering the importance of authigenic output fluxes from the ocean in geochemical cycles.

Generally speaking, the isotopic composition of the so-called diagenetic input flux is a function of the δ value of the carbonate sediment, the δ value of seawater, the diagenetic effect, and relative mass additions or losses in the altered sediment. The relationship between the isotopic composition of the diagenetic flux and these factors can be expressed by considering a system comprised of a reacting solid (*s*), a coexisting pore fluid (*pf*), and an advective flux into ($F_{\text{adv,in}}$) and out of ($F_{\text{adv,out}}$) the pore fluid (Eq. (A1)). Assuming a steady state solid ($F_{\text{precip}} = F_{\text{diss}}$) reservoir and no isotopic fractionation during dissolution ($\alpha_{\text{diss-solid}} = 1$), the isotopic composition of the diagenetic flux (δ_{diag}) is described by a simple mass balance:

$$\delta_{\text{diag}} = \delta_{\text{pf}} = \frac{F_{\text{R}}}{F_{\text{R}} + F_{\text{adv,in}}}(\delta_{\text{s}} - \Delta_{\text{precip-pf}}) + \frac{F_{\text{adv,in}}}{F_{\text{R}} + F_{\text{adv,in}}}\delta_{\text{adv,in}} \quad (5)$$

where F_{R} is the recrystallization flux ($=F_{\text{diss}}=F_{\text{precip}}$) and the isotopic composition of the advective output flux is assumed to be identical to that of the pore fluid ($\delta_{\text{adv,out}} = \delta_{\text{pf}}$). As expected, in the absence of reaction ($F_{\text{R}} = 0$) the isotopic composition of the diagenetic flux is simply equal to the advective input (i.e., seawater). In the presence of reaction ($F_{\text{R}} > 0$), the delta value of the diagenetic flux is altered towards the solid δ value. This is reflected in Fig. 7d, which illustrates the evolution of pore fluid δ^{44}Ca and δ^{26}Mg in the time-dependent box model. What the steady state model suggests, and the time-dependent model illustrates, is that the diagenetic flux can evolve over time as the solid alters, if the entire solid reservoir continually communicates with the pore fluid. This can be seen clearly by recasting Eq. (5) in more relative terms:

$$\delta_{\text{diag}} = \frac{F_{\text{adv,in}}\delta_{\text{adv,in}}}{F_{\text{R}} + F_{\text{adv,in}}}\left[\frac{F_{\text{R}}\delta_{\text{s}}}{F_{\text{adv,in}}\delta_{\text{adv,in}}} + 1\right] \quad (6)$$

assuming $\Delta_{\text{precip-pf}}$ equals zero. As the isotopic composition of the solid approaches that of the advecting fluid ($\delta_{\text{s}} \rightarrow \delta_{\text{adv.in}}$), the leverage to create a unique diagenetic flux diminishes. This is obviously also true if the recrystallization flux is small compared to the advective flux ($\delta_{\text{diag}} \rightarrow \delta_{\text{adv.in}}$).

If the advective input flux is isotopically similar to seawater, diagenesis will generate a diagenetic flux with a delta value lower than that of seawater. The extent of the decrease depends on the balance between the reactive and advective mass fluxes into the pore fluid and degree to which the solid is out of isotopic equilibrium with the pore fluid (δ_{s}–$\Delta_{\text{precip-pf}}$). In the case of Ca, then, the diagenetic flux has the potential to drive seawater δ^{44}Ca to lower values if diagenesis is temporally decoupled from the initial carbonate deposition event.

With regard to Mg, the situation is somewhat different than Ca. The main levers on the temporal evolution of seawater δ^{26}Mg are the riverine/continental weathering flux and the flux of Mg into authigenic dolomite (and perhaps low temperature alteration of oceanic crust/sediments). While the formation of low-Mg carbonates in the water column is an important lever in the Ca cycle, it is not in the Mg cycle.

Given that dolomitization is likely to be decoupled temporally from deposition, it is probably most useful to think about diagenesis as generating a unique input flux rather than altering the output flux on depositional time scales (cf. Eq. (4)). Such a perspective is also useful to adopt because it requires that Mg escapes the diagenetic system in order to be relevant to seawater isotopic evolution. If seawater-derived Mg is quantitatively retained in various authigenic minerals in the sedimentary column, then while important in the evolution of seawater Mg concentration, dolomitization plays no role in the Mg isotopic evolution of seawater.

Interestingly, diagenesis can generate fluxes that can drive seawater δ^{26}Mg either higher or lower, the magnitudes of which are sensitive to the concentration of Mg in the solid, the elemental and isotopic partitioning of Mg into the diagenetic product (K_{Mg} and α^{Mg}_{diag}, respectively), and the advective time scale. Overall, while there is considerable isotopic leverage to alter the δ^{26}Mg of an advecting fluid during carbonate diagenesis (~1‰ to 5‰; Fig. 4), the mass balance is significantly more favorable during dolomitization than limestone diagenesis. Pore fluids can be driven to lower δ^{26}Mg values via dissolution of carbonates, an effect that is enhanced by higher solid Mg concentrations and larger advective time scales. Pore fluids can also be driven to higher δ^{26}Mg values via preferential incorporation of isotopically light Mg into reacting solids (Fig. 8d), an effect that is enhanced by larger advective time scales. The latter effect is primarily associated with dolomitization.

The latter effect is a distillation effect that depends greatly on the relative mass flux of Mg into and out of the pore fluid. Thus dolomitization, which has both mass and isotopic leverage to alter pore fluids ($\alpha \approx 0.998$), can drive advecting fluids (and thus seawater) to substantially higher δ^{26}Mg values (> +0.5‰) compared to limestone diagenesis (see Section 5.2.3). In cases where the mass flux of Mg into the pore fluid via dissolution is small compared to the precipitation flux, limestone diagenesis can drive pore fluids to marginally higher δ^{26}Mg values but the effect is only on the order of 0.1‰.

With regard to the global Mg cycle, if the measured δ^{26}Mg values of dolostone from 1196A are representative of the "global average" δ^{26}Mg value of dolomite precipitated in modern and ancient oceans, then a fractionation factor of about −2‰ is indicated for the formation of dolomite. Given that dolomite is thought to be an important, but variable, component of the global Mg cycle, the existence of such a large fractionation factor suggests that the weathering and/or formation of dolomite is a crucial, if not dominant, lever in determining the δ^{26}Mg of seawater over Earth history. As discussed above, such a lever will only operate if the Mg added to authigenic minerals, ostensibly derived from seawater, is not quantitatively retained in sediments. This feature is certainly testable, requiring spatially resolved characterizations of diagenetic systems from a variety of marine settings.

6. CONCLUSIONS

Metal isotope systems are increasingly employed to reconstruct the past, the interpretations of which constantly confront the boundaries of what is known. Such barriers restrict, and limit, the utility of these novel tools. In particular, given the potential for carbonate diagenesis to impact both the geochemical proxies archived in carbonate sediments and the geochemical cycles of Ca and Mg, understanding and recognizing diagenetic isotope effects in the rock record is crucial.

The isotopic and trace element compositions of platform carbonates from ODP Site 1196A suggest distinct trends associated with limestone diagenesis and dolomitization. The data indicate that marine diagenesis can substantially increase the δ^{44}Ca, and decrease the δ^{26}Mg, values of platform carbonates, while predictably affecting both the carbon and oxygen isotopic compositions (even in the absence of a strong meteoric influence). The multi-isotope, multi-element dataset demonstrates that diagenesis can be fingerprinted, but that multiple tools are necessary to do so. Such tools should allow for constraints to be placed on the extent to which systems can be considered open, which strongly impacts the interpretation of the rock record.

Simple numerical modeling of Ca, Mg, and O isotopes demonstrates that the interpretation of the observed trends as diagenetic is reasonable. The modeling indicates that the Mg distribution coefficient associated with limestone diagenesis is on the order of 1 to $5{\cdot}10^{-3}$. This is about ~15 to 60 times lower than experimental values, and should be preferred over the laboratory value in any model simulating diagenesis in natural systems at low, geologically appropriate diagenetic reaction rates. The modeling also constrains the fractionation factor for Mg associated with dolomitization to be ~0.9980, which is similar to previous empirical estimates.

The current study suggests that diagenesis may play an important role in the geochemical cycles of elements such as Ca and Mg. Depending on the time scale over which diagenesis operates, it can either modify the leverage of the solid in the output flux or generate a distinct input flux to the ocean. Because both mechanisms can affect the evolution of seawater isotopic composition, diagenetic studies in a variety of systems are critical. It is hoped that the framework laid in the current study will aid interpretation in studies of the rock record.

ACKNOWLEDGMENTS

This research used samples and data provided by the Ocean Drilling Program (ODP). M.S.F. thanks Michael Arthur and Dennis Walizer for assistance with the C and O isotope analyses at Penn State, and Donald J. DePaolo for supporting the Ca isotope analyses at the Center for Isotope Geochemistry at UC Berkeley. The authors thank Edward Tipper, as well as two anonymous reviewers, for constructive comments that improved the manuscript.

APPENDIX A.

A.1. Recrystallization box model

A time-dependent box model is used to simulate the effects of diagenetic alteration on the Ca and Mg isotopic composition of the solid. The objectives of the modeling

are (1) to demonstrate the feasibility of explaining the measured trends by invoking diagenesis, and (2) to illustrate the impact of important parameters on the model outcomes. Accordingly, a range of reasonable assumptions regarding the initial chemical and isotopic composition of the solid are made in order to accomplish these objectives.

The equations that describe the time-dependent isotopic evolution of the pore fluid (*pf*) and solid (*s*), derived from first principles, are:

$$\frac{dr_{pf}}{dt} = \frac{F_{diss}}{N_{pf}}(\alpha_{diss-s} r_s - r_{pf}) + \frac{F_{adv,in}}{N_{pf}}(r_{adv,in} - r_{pf}) + \frac{F_{precip}}{N_{pf}} r_{pf}(1 - \alpha_{precip-pf}) + \frac{F_{adv,out}}{N_{pf}}(r_{pf} - r_{adv,out}) \quad (A1)$$

and:

$$\frac{dr_s}{dt} = \frac{F_{precip}}{N_s}(\alpha_{precip-pf} r_{pf} - r_s) + \frac{F_{diss}}{N_s} r_s (1 - \alpha_{diss-s}) \quad (A2)$$

where "*diss*" refers to the dissolution flux into the pore fluid, "*precip*" refers to the precipitation flux into the solid, and "*adv*" refers to the advection flux either into ("*in*") or out of ("*out*") the pore fluid. In all equations, "*F*" refers to a mass flux in moles per time, "*N*" indicates a mass of a reservoir (moles), and "*r*" is the isotope ratio of either Ca ($^{44}Ca/^{40}Ca$) or Mg ($^{26}Mg/^{24}Mg$). It is important to note that the solid is considered to be a single, homogeneous reservoir in the model approach taken. Thus, the pore fluid is influenced by reaction with the bulk solid, and not only the primary solid, over the course of the simulation. In the equations above, the fractionation factors (α_i) are generally defined by:

$$\alpha_{precip-pf} = \frac{r_{precip}}{r_{pf}} \quad (A3)$$

and

$$\alpha_{diss-s} = \frac{r_{diss}}{r_s} \quad (A4)$$

In all simulations presented herein, and with respect to both Ca and Mg, the fractionation factor associated with dissolution is always assumed to equal 1. The fractionation factor associated with precipitation of Ca is also assigned a value of 1, based on previous work in deep-sea nannofossil ooze (Fantle and DePaolo, 2007). Such an assumption is not critical to the modeling, as long as the fractionation factor associated with diagenesis is substantially closer to 1 than that associated with formation in the surface ocean. The fractionation factor associated with precipitation of Mg is assigned a value of 0.9955 (−4.5‰), based primarily on *ab initio* numerical modeling (Rustad et al., 2010; Schauble, 2011). In both cases, the fractionation factor and pore fluid isotopic composition define the isotopic composition of the diagenetic endmember. Thus, changing either (or both) quantities will affect the model trajectories.

The mass evolution of the solid (*s*) and pore fluid (*pf*) reservoirs in the model is described by:

$$\frac{dN_s}{dt} = F_{precip} - F_{diss} \quad (A5)$$

and

$$\frac{dN_{pf}}{dt} = F_{diss} + F_{adv,in} - F_{precip} - F_{adv,out} \quad (A6)$$

The mass flux associated with advection is parametrized by assigning an advective time scale (τ_{adv}) for the pore fluid reservoir, which describes the time scale over which the fluid in the pore fluid reservoir is replaced. Using this time scale, the corresponding model fluid flux is calculated (*Q*, cm^3/time):

$$Q_{adv} = \frac{V_{fluid}}{\tau_{adv}} = \frac{\phi \cdot V_{total}}{\tau_{adv}} \quad (A7)$$

where *V* is the volume occupied by the fluid (cm^3) and ϕ is the porosity (=constant in time). The elemental flux for either Ca or Mg is $Q_{adv} \cdot [X]_{fluid}$ in units of moles of element *X* per time. In the case of advection into the pore fluid reservoir, the chemistry of modern seawater determines the advecting fluid endmember ($[Ca^{2+}] = 10.3$ mM, $[Mg^{2+}] = 52$ mM, $\delta^{44}Ca = 1.95‰$, and $\delta^{26}Mg = -0.8‰$); in the case of advection out of the pore fluid reservoir, the modeled pore fluid chemistry is used with no elemental or isotopic fractionation. The initial model fluid composition is not necessarily identical to the advecting endmember, but is dictated by the balance between the reactive (F_{precip} and F_{diss}) and advective (F_{adv}) fluxes. This initial fluid is calculated prior to each run and the appropriate initial $\delta^{44}Ca$ and $\delta^{26}Mg$ values assigned.

In all simulations, the porosity (ϕ) is 0.4 and the solid is modeled as a single, homogeneous reservoir. Unless otherwise noted, τ_{adv} is assigned a value of 25; this parameter is varied to a maximum value of 1000 in a subset of the simulations presented, and to 2000 in simulations not presented. In the case of limestone diagenesis, using a value of 25 for τ_{adv} provides maximum isotopic leverage to alter $\delta^{26}Mg$ and slightly less than maximum leverage to alter $\delta^{44}Ca$ (Fig. 7d). The necessity of using this value of τ_{adv} as a reference is borne from numerical instability in the model at $dt = 25$ when τ_{adv} is order ~1. In order to simulate over the total times desired, we increased τ_{adv} so that we could perform the runs in a reasonable amount of time. Such an approach is, we believe, sufficient for conveying the feasibility of the preferred interpretation. In the one simulation where $\tau_{adv} = 5$ (Fig. 7d), *dt* was lowered to 5 and the total simulation time increased markedly.

The dissolution rate of the solid reservoir is constant in time in all simulations (*units*: $time^{-1}$; mass reacted/mass solid/time). In the case of limestone diagenesis, the Ca dissolution and precipitation fluxes are set to be equal, while the Mg dissolution and precipitation fluxes are determined by:

$$F^{Mg}_{diss} = \frac{N^{Mg}_{solid}}{N^{Ca}_{solid}} \cdot F^{Ca}_{diss} \quad (A8)$$

$$F^{Mg}_{precip} = K_{Mg} \frac{N^{Mg}_{pf}}{N^{Ca}_{pf}} F^{Ca}_{precip} \quad (A9)$$

The parameter K_{Mg} is the distribution coefficient for $Mg = (N^{solid}_{Mg}/N^{solid}_{Ca})/(N^{fluid}_{Mg}/N^{fluid}_{Ca})$, which is held constant in time in all limestone simulations. In all simulations, the time dependent equations are solved using Euler's method ($dt = 25$ units), and run for ⩾300,000 time units. Due to memory constraints, the simulations are not run to complete isotopic equilibrium ($\delta^{44}Ca_{solid} = 1.95‰$, $\delta^{26}Mg_{solid} = -5.3‰$).

To simulate dolomitization, a one-box approach is also utilized in which the dissolution flux is constant in time. In this formulation, the Ca mass loss from the solid phase is balanced by Mg gain on a mole for mole basis. Accordingly mass balance considerations dictate that the precipitation flux of Ca into the solid is constrained by:

$$F^{Ca}_{precip} = \frac{F^{Ca}_{diss} + F^{Mg}_{diss}}{1 + K_{Mg}\frac{N^{Mg}_{pf}}{N^{Ca}_{pf}}} \quad (A10)$$

which assumes that $N^{Ca}_{solid} + N^{Mg}_{solid} =$ constant and, thus, that $dN^{Ca}_{solid}/dt = -dN^{Mg}_{solid}/dt$. The distribution coefficient for Mg is assigned a time-independent value of 0.2 in most dolomitization simulations (Fig. 8c). However, in a subset of dolomitization simulations, the K_{Mg} value is varied in time in concert with the pore fluid Mg/Ca ratio, so that the precipitation flux always has a Mg/Ca molar ratio of 1 mol:1 mol (Fig. 8d).

The coupled Ca–Mg–O isotope dolomitization model is similar in all respects to those described above. The Ca mass flux into the solid is related to the precipitation fluxes of Ca and Mg, such that the O/(Ca + Mg) of the flux into the solid is 3:1 [i.e., eventually forming stoichiometric dolomite: $CaMg(CO_3)_2$]. The mass of oxygen in the solid phase, in addition to the mass of (Ca + Mg), is constant in the model.

The oxygen isotopic fractionation factor associated with dolomitization is extrapolated from the equation of Horita (2014):

$$10^3 \ln \alpha_{dolomite-water} = \frac{3.14 \cdot 10^6}{T^2(K)} - 3.14 \quad (A11)$$

This equation is strictly valid only to a lower temperature limit of 80 °C, but is used as the best available estimate of equilibrium oxygen isotopic fractionation at low temperatures. For the range of temperatures investigated, the extrapolated fractionation factors are 1.0374 (7.5 °C), 1.0360 (12.5 °C), and 1.0346 (17.5 °C). All Ca–Mg–O models were run for 400,000 time units ($dt = 25$) at the same reaction rates as all other models, in order to cover the range of oxygen isotope space desired.

REFERENCES

Anderson T. F. and Arthur M. A. (1983) Stable isotopes of oxygen and carbon and their applications to sedimentologic and paleoenvironmental problems. In *Stable Isotopes in Sedimentary Geology*, Vol. SEPM Short Course, 10 (eds. M.A. Arthur, T.F. Anderson, I.F. Kaplan, et al.). pp. 1–151.

Baker P. A., Gieskes J. M. and Elderfield H. (1982) Diagenesis of carbonates in deep-sea sediments: Evidence from Sr/Ca ratios and interstitial dissolved Sr^{2+} data. *J. Sediment. Petrol.* **52**, 71–82.

Baker P. A. and Kastner M. (1981) Constraints on the formation of sedimentary dolomite. *Science* **213**(4504), 214–216. http://dx.doi.org/10.1126/science.213.4504.214.

Berggren W. A. (1995) *Geochronology, time scales, and global stratigraphic correlation: Tulsa*. SEPM (Society for Sedimentary Geology), OK, 386 p.

Blattler C. L., Henderson G. M. and Jenkyns H. C. (2012) Explaining the phanerozoic Ca isotope history of seawater. *Geology* **40**, 843–846 (9, doi:10.1130/G33191.1).

Böhm F., Gussone N., Eisenhauer A., Dullo W. C., Reynaud S. and Paytan A. (2006) Calcium isotope fractionation in modern scleractinian corals. *Geochim. Cosmochim. Acta* **70**(17), 4452–4462.

Boyle R. (1674) Observations and Experiments about the Saltness of the Sea.

Broecker W. S. (1971) A kinetic model for the chemical composition of sea water. *Quat. Res.* **1**(2), 188–207.

Capo R. C. and DePaolo D. J. (1990) Seawater strontium isotopic variations from 2.5 million years ago to the present. *Science* **249**(4964), 51–55.

Chacko T. and Deines P. (2008) Theoretical calculation of oxygen isotope fractionation factors in carbonate systems. *Geochim. Cosmochim. Acta* **72**(15), 3642–3660.

Chang V. T. C., Williams R. J. P., Makishima A., Belshawl N. S. and O'Nions R. K. (2004) Mg and Ca isotope fractionation during $CaCO_3$ biomineralisation. *Biochem. Biophys. Res. Commun.* **323**(1), 79–85.

Clarke F. W. (1911) *The Data of Geochemistry*. The Government Printing Office, Washington, D.C..

Clayton R. N., Jones B. F. and Berner R. A. (1968) Isotope studies of dolomite formation under sedimentary conditions. *Geochim. Cosmochim. Acta* **32**(4), 415.

Conesa G. R. A., Favre E., Münch P., Dalmasso H. and Chaix C. (2005) Biosedimentary and paleoenvironmental evolution of the Southern Marion Platform from the middle to late Miocene (northeast Australia, ODP Leg 194, Sites 1196 and 1199). In *Proceedings of the Ocean Drilling Project, Scientific Results*, Vol. 194, doi:10.2973/odp.proc.sr.194.005.2005 (eds. F.S. Anselmetti, A.R Isern, P. Blum, et al.), pp. 1–38 (Ocean Drilling Program).

Conway E. J. (1943) The chemical evolution of the ocean. *Proc. R. Irish Acad.* **48B**(8), 161–212.

Craig H. (1957) Isotopic standards for carbon and oxygen and correction factors for mass-spectrometric analysis of carbon dioxide. *Geochim. Cosmochim. Acta* **12**, 133–149.

De La Rocha C. L. and DePaolo D. J. (2000) Isotopic evidence for variations in the marine calcium cycle over the Cenozoic. *Science* **289**(5482), 1176–1178.

Deines P. (2004) Carbon isotope effects in carbonate systems. *Geochim. Cosmochim. Acta* **68**(12), 2659–2679.

DePaolo D. J. (1986) Detailed record of the Neogene Sr isotopic evolution of seawater from DSDP Site 590B. *Geology* **14**(2), 103–106.

DePaolo D. J. (2004) Calcium isotopic variations produced by biological, kinetic, radiogenic, and nucleosynthetic processes. In *Geochemistry of non-Traditional Stable Isotopes*, Vol. 55 (eds. C.M. Johnson, B.L. Beard, F. Albarede). pp. 255–288 (Mineralogical Society of America; Geochemical Society).

DePaolo D. J. and Ingram B. L. (1985) High-resolution stratigraphy with strontium isotopes. *Science* **227**(4689), 938–941.

Ehrenberg S. N., Eberli G. P. and Baechle G. (2006a) Porosity-permeability relationships in Miocene carbonate platforms and slopes seaward of the Great Barrier Reef, Australia (ODP Leg 194, Marion Plateau). *Sedimentology* **53**(6), 1289–1318.

Ehrenberg S. N., McArthur J. M. and Thirlwall M. F. (2006b) Growth, demise, and dolomitization of Miocene carbonate platforms on the Marion Plateau, offshore NE Australia. *J. Sediment. Res.* **76**(1–2), 91–116.

Fantle M. S. (2010) Evaluating the Ca isotope proxy. *Am. J. Sci.* **310**, 194–230, doi 10.2475/03.2010.03.

Fantle M. S. and Bullen T. D. (2009) Essentials of iron, chromium, and calcium isotope analysis of natural materials by thermal ionization mass spectrometry. *Chem. Geol.* **258**(1–2), 50–64.

Fantle M. S. and DePaolo D. J. (2005) Variations in the marine Ca cycle over the past 20 million years. *Earth Planet. Sci. Lett.* **237**(1–2), 102–117.

Fantle M. S. and DePaolo D. J. (2006) Sr isotopes and pore fluid chemistry in carbonate sediment of the Ontong Java Plateau: calcite recrystallization rates and evidence for a rapid rise in seawater Mg over the last 10 million years. *Geochim. Cosmochim. Acta* **70**(15), 3883–3904.

Fantle M. S. and DePaolo D. J. (2007) Ca isotopes in carbonate sediment and pore fluid from ODP Site 807A: the Ca^{2+}(aq)-calcite equilibrium fractionation factor and calcite recrystallization rates in Pleistocene sediments. *Geochim. Cosmochim. Acta* **71**(10), 2524–2546.

Fantle M. S., Maher K. M. and DePaolo D. J. (2010) Isotopic approaches for quantifying the rates of marine burial diagenesis. *Rev. Geophys.* **48**, RG3002, doi:10.1029/2009RG000306.

Fantle M. S. and Teng F.-Z. (2012) Evaluating pore fluid Mg isotopic and elemental constraints on seawater Mg chemistry in the Cenozoic. *Mineral. Mag.* **76**(6), 1692–1728.

Fantle M. S. and Tipper E. T. (2014) Calcium isotopes in the global biogeochemical Ca cycle: implications for development of a Ca isotope proxy. *Earth-Sci. Rev.* **129**, 148–177, http://dx.doi.org/10.1016/j.earscirev.2013.10.004.

Farkaš J., Böhm F., Wallmann K., Blenkinsop J., Eisenhauer A., van Geldern R., Munnecke A., Voigt S. and Veizer J. (2007) Calcium isotope record of Phanerozoic oceans: implications for chemical evolution of seawater and its causative mechanisms. *Geochim. Cosmochim. Acta* **71**(21), 5117–5134.

Fritz P. and Smith D. G. W. (1970) Isotopic composition of secondary dolomites. *Geochim. Cosmochim. Acta* **34**(11), 1161–1173.

Galy A., Belshaw N. S., Halicz L. and O'Nions R. K. (2001) High-precision measurement of magnesium isotopes by multiple-collector inductively coupled plasma mass spectrometry. *Int. J. Mass Spectrom.* **208**(1–3), 89–98.

Graham D. W., Bender M. L., Williams D. F. and Keigwin L. D. (1982) Strontium-calcium ratios in cenozoic planktonic foraminifera. *Geochim. Cosmochim. Acta* **46**(7), 1281–1292.

Gussone N., Böhm F., Eisenhauer A., Dietzel M., Heuser A., Teichert B. M. A., Reitner J., Worheide G. and Dullo W. C. (2005) Calcium isotope fractionation in calcite and aragonite. *Geochim. Cosmochim. Acta* **69**(18), 4485–4494.

Gussone N. and Filipsson H. L. (2010) Calcium isotope ratios in calcitic tests of benthic foraminifers. *Earth Planet. Sci. Lett.* **290**(1–2), 108–117.

Halicz L., Galy A., Belshaw N. S. and O'Nions R. K. (1999) High-precision measurement of calcium isotopes in carbonates and related materials by multiple collector inductively coupled plasma mass spectrometry (MC-ICP-MS). *J. Anal. At. Spectrom.* **14**(12), 1835–1838.

Halley E. (1714) A short account of the cause of the saltness of the ocean, and of the several lakes that emit no rivers; with a proposal, by help thereof, to discover the age of the world. *Phil. Trans. R. Soc. Lond.* **29**, 296–300, doi: 10.1098/rstl.1714.0031.

Hess J., Bender M. L. and Schilling J. G. (1986) Evolution of the ratio of Sr-87 to Sr-86 in seawater from Cretaceous to present. *Science* **231**(4741), 979–984.

Higgins J. A. and Schrag D. P. (2010) Constraining magnesium cycling in marine sediments using magnesium isotopes. *Geochim. Cosmochim. Acta* **74**(17), 5039–5053.

Higgins J. A. and Schrag D. P. (2012) Records of Neogene seawater chemistry and diagenesis in deep-sea carbonate sediments and pore fluids. *Earth Planet. Sci. Lett.* **357**, 386–396.

Hippler D., Witbaard R., van Aken H. M., Buhl D. and Immenhauser A. (2011) Exploring the calcium isotope signature of Arctica islandica as an environmental proxy using laboratory- and field-cultured specimens. *Palaeogeogr. Palaeoclimatol. Palaeoecol.*. http://dx.doi.org/10.1016/j.palaeo.2011.11.015.

Holland H. D. (1965) The history of ocean water and its effect on the chemistry of the atmosphere. *SYMPOSIUM ON THE EVOLUTION OF THE EARTH'S ATMOSPHERE: Proceedings of the National Academy of Sciences of the United States of America* **53**(6), 1173–1183.

Holland H. D. (2005) Sea level, sediments and the composition of seawater. *Am. J. Sci.* **305**(3), 220–239.

Holmden C. (2005) Measurement of δ^{44}Ca using a ^{42}Ca–^{43}Ca double-spike TIMS technique. *Summ. Invest. Sask. Ind. Resour. Misc. Rep.*, 1–7.

Holmden C. (2009) Ca isotope study of Ordovician dolomite, limestone, and anhydrite in the Williston Basin: implications for subsurface dolomitization and local Ca cycling. *Chem. Geol.* **268**(3–4), 180–188.

Holmden C., Papanastassiou D. A., Blanchon P. and Evans S. (2012) $\Delta^{44/40}$Ca variability in shallow water carbonates and the impact of submarine groundwater discharge on Ca-cycling in marine environments. *Geochim. Cosmochim. Acta* **83**, 179–194. http://dx.doi.org/10.1016/j.gca.2011.12.031.

Horita J. (2014) Oxygen and carbon isotope fractionation in the system dolomite-water-CO_2 to elevated temperatures. *Geochim. Cosmochim. Acta* **129**, 111–124.

Hut G. (1987) *Consultants' Group Meeting on Stable Isotope Reference Samples for Geochemical and Hydrological Investigations*. IAEA, Vienna, Austria, 16–18 September, 1985.

IODP. (2014) IODP-USIO: Log database http://iodp.ldeo.columbia.edu/DATA/.

Isern, Alexandra R., Anselmetti, Flavio S., Blum, Peter, Andresen, Nils, Birke, Tesfaye Kidane, Bracco Gartner, Guido L., Burns, Stephen J., Conesa, Gilles A. R., Delius, Heike, Dugan, Brandon, Eberli, Gregor P., Ehrenberg, Stephen, Fuller, Michael D., Muller, Pamela Hallock, Hine, Albert C., Howell, Michael W., John, Cedric M., Karner, Garry D., Kindler, Pascal F., Olson, Brooke E., Sasaki, Keiichi, Stewart, Duncan, Wei, Wuchang, White, Timothy S., Wood, Jason L., Yamada, Tsutomu, and Ocean Drilling Program, Leg 194, Shipboard Scientific Party (2002) Sites 1196 and 1199. In *Proceedings of the Ocean Drilling Program: Initial reports*, Vol. 194 (eds. A.R. Isern, F.S. Anselmetti, P. Blum, et al.), pp. 1–149, doi:10.2973/odp.proc.ir.194.107.2002. Texas A&M University (Ocean Drilling Program).

Jacobson A. D. and Holmden C. (2008) Δ^{44}Ca evolution in a carbonate aquifer and its bearing on the equilibrium isotope fractionation factor for calcite. *Earth Planet. Sci. Lett.* **270**(3–4), 349–353.

Joly J. (1899) An estimate of the geological age of the Earth. *The Scientific Transactions of the Royal Dublin Society* **VII, Series II**, 23–66.

Kasemann S. A., Hawkesworth C. J., Prave A. R., Fallick A. E. and Pearson P. N. (2005) Boron and calcium isotope composition in Neoproterozoic carbonate rocks from Namibia: evidence for extreme environmental change. *Earth Planet. Sci. Lett.* **231**(1–2), 73–86.

Katz A. (1973) Interaction of magnesium with calcite during crystal growth at 25 °C and one atmosphere. *Geochim. Cosmochim. Acta* **37**(6), 1563–1586.

Kennett James P. (1986) Miocene to early Pliocene oxygen and carbon isotope stratigraphy in the Southwest Pacific, Deep Sea Drilling Project Leg 90. In *Initial reports of the Deep Sea Drilling Project covering Leg 90 of the cruises of the drilling vessel Glomar Challenger; Noumea, New Caledonia, to Welling-*

ton, New Zealand, December 1982-January 1983; Part 1, Vol. 90 (ed. J.H. Blakeslee). pp. 1383–1411 (U.S. Govt. Printing Office).

Knauth L. P. and Kennedy M. J. (2009) The late Precambrian greening of the Earth. *Nature* **460**(7256), 728–732.

Komiya T., Suga A., Ohno T., Han J., Guo J. F., Yamamoto S., Hirata T. and Li Y. (2008) Ca isotopic compositions of dolomite, phosphorite and the oldest animal embryo fossils from the Neoproterozoic in Weng'an, South China. *Gondwana Res.* **14**(1–2), 209–218.

Krause S., Liebetrau V., Gorb S., Sanchez-Roman M., McKenzie J. A. and Treude T. (2012) Microbial nucleation of Mg-rich dolomite in exopolymeric substances under anoxic modern seawater salinity: new insight into an old enigma. *Geology* **40**(7), 587–590.

Land L. S. (1980) The isotopic and trace element geochemistry of dolomite: the state of the art. *SEPM Spec. Publ.* **28**, 87–110.

Langer G., Gussone N., Nehrke G., Riebesell U., Eisenhauer A. and Thoms S. (2007) Calcium isotope fractionation during coccolith formation in Emiliania huxleyi: independence of growth and calcification rate. *Geochem. Geophys. Geosys.* **8**(Q05007). http://dx.doi.org/10.1029/2006GC001422.

Ling M. X., Sedaghatpour F., Teng F. Z., Hays P. D., Strauss J. and Sun W. D. (2011) Homogeneous magnesium isotopic composition of seawater: an excellent geostandard for Mg isotope analysis. *Rapid Commun. Mass Spectrom.* **25**(19), 2828–2836.

Mackenzie F. T. and Morse J. W. (1992) Sedimentary carbonates through phanerozoic time. *Geochim. Cosmochim. Acta* **56**(8), 3281–3295.

Maher K., DePaolo D. J. and Lin J. C. F. (2004) Rates of silicate dissolution in deep-sea sediment: in situ measurement using $^{234}U/^{238}U$ of pore fluids. *Geochim. Cosmochim. Acta* **68**(22), 4629–4648.

Maher K., Steefel C. I., DePaolo D. J. and Viani B. E. (2006) The mineral dissolution rate conundrum: insights from reactive transport modeling of U isotopes and pore fluid chemistry in marine sediments. *Geochim. Cosmochim. Acta* **70**(2), 337–363.

Malone M. (2000) Data Report: Geochemistry and mineralogy of periplatform carbonate sediments: Sites 1006, 1008, and 1009. In *Proceedings of the Ocean Drilling Program, Scientific Results*, Vol. 166, doi:10.2973/odp.proc.sr.166.125.2000 (eds. P.K. Swart, G.P. Eberli, M.J. Malone, et al.). pp. 145–152 (Ocean Drilling Program).

Malone M. J., Baker P. A. and Burns S. J. (1996) Recrystallization of dolomite: an experimental study from 50–200C. *Geochim. Cosmochim. Acta* **60**(12), 2189–2207.

Mavromatis V., Gautier Q., Bosc O. and Schott J. (2013) Kinetics of Mg partition and Mg stable isotope fractionation during its incorporation in calcite. *Geochim. Cosmochim. Acta* **114**, 188–203.

McArthur J. M. and Howarth R. J. (2004) Strontium isotope stratigraphy. In *A Geological Timescale 2004* (eds. J. Ogg, F. Gradstein and A. Smith). Cambridge University Press, pp. 96–105.

Milliman J. D. (1974) *Recent Sedimentary Carbonates: Pt 1. Marine Carbonate*. .

Mitsuguchi T., Uchida T. and Matsumoto E. (2010) Na/Ca variability in coral skeletons. *Geochem. J.* **44**(4), 261–273.

Nägler T. F., Eisenhauer A., Müller A., Hemleben C. and Kramers J. (2000) The δ^{44}Ca-temperature calibration on fossil and cultured Globigerinoides sacculifer: new tool for reconstruction of past sea surface temperatures. *Geochem. Geophys. Geosyst.* **1**, 2000GC000091.

Northrop D. A. and Clayton R. N. (1966) Oxygen-isotope fractionations in systems containing dolomite. *J. Geol.* **74**(2), 174.

Oomori T., Kaneshima H., Maezato Y. and Kitano Y. (1987) Distribution coefficient of Mg^{2+} ions between calcite and solution at 10–50 °C. *Mar. Chem.* **20**(4), 327–336.

Pretet C., Samankassou E., Felis T., Reynaud S., Böhm F., Eisenhauer A., Ferrier-Pages C., Gattuso J. P. and Camoin G. (2013) Constraining calcium isotope fractionation (delta Ca-44/40) in modern and fossil scleractinian coral skeleton. *Chem. Geol.* **340**, 49–58.

Richter F. M. (1996) Models for the coupled Sr-sulfate budget in deep-sea carbonates. *Earth Planet. Sci. Lett.* **141**(1–4), 199–211.

Richter F. M. and DePaolo D. J. (1987) Numerical models for diagenesis and the Neogene Sr isotopic evolution of seawater from DSDP Site 590B. *Earth Planet. Sci. Lett.* **83**(1–4), 27–38.

Richter F. M. and DePaolo D. J. (1988) Diagenesis and Sr isotopic evolution of seawater using data from DSDP-590B and DSDP-575. *Earth Planet. Sci. Lett.* **90**(4), 382–394.

Richter F. M. and Liang Y. (1993) The rate and consequences of Sr diagenesis in deep-sea carbonates. *Earth Planet. Sci. Lett.* **117**(3–4), 553–565.

Rosenbaum J. and Sheppard S. M. F. (1986) An isotopic study of siderites, dolomites and ankerites at high-temperatures. *Geochim. Cosmochim. Acta* **50**(6), 1147–1150.

Rubey W. W. (1951) Geologic history of seawater: an attempt to state the problem. *Geol. Soc. Am. Bull.* **62**, 1111–1148.

Rustad J. R., Casey W. H., Yin Q. Z., Bylaska E. J., Felmy A. R., Bogatko S. A., Jackson V. E. and Dixon D. A. (2010) Isotopic fractionation of Mg2+(aq), Ca2+(aq), and Fe2+(aq) with carbonate minerals. *Geochim. Cosmochim. Acta* **74**(22), 6301–6323.

Schauble E. A. (2011) First-principles estimates of equilibrium magnesium isotope fractionation in silicate, oxide, carbonate and hexaaquamagnesium(2+) crystals. *Geochim. Cosmochim. Acta* **75**(3), 844–869.

Schauble E. A., Ghosh P. and Eiler J. M. (2006) Preferential formation of C-13–O-18 bonds in carbonate minerals, estimated using first-principles lattice dynamics. *Geochim. Cosmochim. Acta* **70**(10), 2510–2529.

Schmidt M., Xeflide S., Botz R. and Mann S. (2005) Oxygen isotope fractionation during synthesis of CaMg-carbonate and implications for sedimentary dolomite formation. *Geochim. Cosmochim. Acta* **69**(19), 4665–4674.

Shackleton N. J., Hall M. A. and Boersma A. (1984) Oxygen and carbon isotope data from Leg-74 Foraminifers. *Init. Rep. Deep Sea Drilling Proj.* **74**(MAR), 599–612.

Sharma T. and Clayton R. N. (1965) Measurement of O18/O16 ratios of total oxygen of carbonates. *Geochim. Cosmochim. Acta* **29**(12), 1347–1353.

Sheppard S. M. and Schwarcz H. P. (1970) Fractionation of carbon and oxygen isotopes and magnesium between coexisting metamorphic calcite and dolomite. *Contrib. Miner. Petrol.* **26**(3), 161–198.

Sillen L. G. (1961) The Physical Chemistry of Seawater. In *Oceanography: Invited lectures presented at the International Oceanographic Congress, New York, 1959*, Vol. no. 67 (ed. M. Sears). pp. 549–581 (American Association for the Advancement of Science Publication).

Sillen L. G. (1963) How has seawater got its present composition? *Sven. Kem. Tidskr.* **75**(4), 161–177.

Sime N. G., De La Rocha C. L., Tipper E. T., Tripati A., Galy A. and Bickle M. J. (2007) Interpreting the Ca isotope record of marine biogenic carbonates. *Geochim. Cosmochim. Acta* **71**(16), 3979–3989.

Simon J. I. and DePaolo D. J. (2010) Stable calcium isotopic composition of meteorites and rocky planets. *Earth Planet. Sci. Lett.* **289**(3–4), 457–466.

Simon J. I., DePaolo D. J. and Moynier F. (2009) Calcium isotope composition of meteorites, earth, and mars. *Astrophys. J.* **702**(1), 707–715.

Swart P. K., Burns S. J. and Leder J. J. (1991) Fractionation of the stable isotopes of oxygen and carbon in carbon dioxide during the reaction of calcite with phosphoric acid as a function of temperature and technique. *Chem. Geol.* **86**, 89–96.

Swart P. K., Isern A. R., Elderfield H. and McKenzie J. A. (1993) A summary of interstitial water geochemistry of Leg 133. In *Proceedings of the Ocean Drilling Program, Scientific Results*, Vol. 133, doi:10.2973/odp.proc.sr.133.258.1993 (ed. J.A. McKenzie, P.J. Davies and A. Palmer-Julson, et al.). pp. 705–721 (Ocean Drilling Program).

Swart P. K. and Melim L. A. (2000) The origin of dolomites in tertiary sediments from the margin of Great Bahama Bank. *J. Sediment. Res.* **70**(3), 738–748.

Tang J. W., Dietzel M., Böhm F., Kohler S. J. and Eisenhauer A. (2008) Sr^{2+}/Ca^{2+} and $^{44}Ca/^{40}Ca$ fractionation during inorganic calcite formation: II. Ca isotopes. *Geochim. Cosmochim. Acta* **72**(15), 3733–3745.

Tang J. W., Niedermayr A., Kohler S. J., Böhm F., Kisakurek B., Eisenhauer A. and Dietzel M. (2012) Sr^{2+}/Ca^{2+} and Ca-44/Ca-40 fractionation during inorganic calcite formation: III. Impact of salinity/ionic strength. *Geochim. Cosmochim. Acta* **77**, 432–443.

Tipper E. T., Galy A. and Bickle M. J. (2008) Calcium and magnesium isotope systematics in rivers draining the Himalaya-Tibetan-Plateau region: lithological or fractionation control? *Geochim. Cosmochim. Acta* **72**(4), 1057–1075.

Tipper E. T., Galy A., Gaillardet J., Bickle M. J., Elderfield H. and Carder E. A. (2006) The magnesium isotope budget of the modern ocean: Constraints from riverine magnesium isotope ratios. *Earth Planet. Sci. Lett.* **250**, 241–253.

Turchyn A. V. and DePaolo D. J. (2011) Calcium isotope evidence for suppression of carbonate dissolution in carbonate-bearing organic-rich sediments. *Geochim. Cosmochim. Acta* **75**, 7081–7098.

Walker John. and Scott Harold. W. (1966) *Lectures on Geology, Including Hydrography, Mineralogy, and Meteorology, with an Introduction to Biology*. University of Chicago Press, Chicago.

Watkins J. M., Nielsen L. C., Ryerson F. J. and DePaolo D. J. (2013) The influence of kinetics on the oxygen isotope composition of calcium carbonate. *Earth Planet. Sci. Lett.* **375**, 349–360.

Wombacher F., Eisenhauer A., Böhm F., Gussone N., Regenberg M., Dullo W. C. and Ruggeberg A. (2011) Magnesium stable isotope fractionation in marine biogenic calcite and aragonite. *Geochim. Cosmochim. Acta* **75**(19), 5797–5818.

Zachos J., Pagani M., Sloan L., Thomas E. and Billups K. (2001) Trends, rhythms, and aberrations in global climate 65 Ma to present. *Science* **292**(5517), 686–693.

Associate editor: Andrew Ross Bowie